Serhat YANIK

M.S. Thesis in Physics

July - 2011

PREPARATION AND CHARACTERIZATION OF GRAPHENE SAMPLES ON ATOMICALLY SMOOTH SURFACES

by

Serhat YANIK

July 2011

PREPARATION AND CHARACTERIZATION OF GRAPHENE SAMPLES ON ATOMICALLY SMOOTH SURFACES

by

Serhat YANIK

July 2011

PREPARATION AND CHARACTERIZATION OF GRAPHENE SAMPLES ON ATOMICALLY SMOOTH SURFACES

by

Serhat YANIK

A thesis submitted to

the Graduate Institute of Sciences and Engineering

of

Fatih University

in partial fulfillment of the requirements for the degree of

Master of Science

in

Physics

July 2011
Istanbul, Turkey

APPROVAL PAGE

I certify that this thesis satisfies all the requirements as a thesis for the degree of Master of Science.

Prof. Mustafa KUMRU
Head of Department

This is to certify that I have read this thesis and that in my opinion it is fully adequate, in scope and quality, as a thesis for the degree of Master of Science.

Assist. Prof. Mehmet
Burak YILMAZ
Supervisor

Examining Committee Members

Assist. Prof. Mehmet Burak YILMAZ ……..

Assoc. Prof. Kurtuluş Gölcük …….

Assist. Prof. Burak Esat ……..

It is approved that this thesis has been written in compliance with the formatting rules laid down by the Graduate Institute of Sciences and Engineering.

Assoc. Prof. Nurullah ARSLAN
Director

PREPARATION AND CHARACTERIZATION OF GRAPHENE SAMPLES ON ATOMICALLY SMOOTH SURFACES

Serhat YANIK

M. S. Thesis –Physics
July 2011

Supervisor: Assist. Prof. Mehmet Burak YILMAZ

ABSTRACT

Graphene is a two dimensional carbon monolayer of graphite arranged in a honeycomb lattice. Recent experimental advances have allowed researchers to isolate monolayer and multilayer graphene samples by micro-mechanical cleavage (that is exfoliation from graphite) [1] and epitaxial growth [2]. While micro-mechanical cleavage is performed on SiO_2/Si surfaces, epitaxial growth has been achieved on SiC and some metal surfaces. These developments have caused a sudden burst in experimental and theoretical research attention. Much of the interest in graphene derives from the similarity of the energy-momentum relationship of the electrons about to K point in the momentum space to that of relativistic, massless fermions. This peculiar band structure leads to intriguing new phenomena. For instance, a very unusual half-integer quantum Hall effect (QHE) and a non-zero Berry's phase have been discovered in graphene [3,4] and recent photoemission work on this material has revealed interesting features in the electronic structure [5-7].

In this work we have performed Raman and AFM study of graphene samples obtained through exfoliation method on both SiO_2 and mica substrates. The Raman and AFM measurements performed on SiO_2 surfaced were consistent with previous work done on the same substrate. Mica substrates are atomically smooth for large areas and as a result graphene exfoliated on mica also does not have any roughness. We have compared the Raman spectra from graphene on mica and on SiO_2 and observed that unlike graphene on SiO_2, there is no variation in the 2D-mode Raman peak position for graphene on mica. Such variations are attributed to doping of the sample by the charged impurities. Our result indicates that impurity doping of the atomically smooth graphene is uniform throughout the sample. In AFM measurements in addition to use contact mode AFM for thickness measurements of graphene, we also used lateral force microscopy (LFM) to obtain frictional properties of graphene relative to that of mica. We found that frictional forces on graphene is approximately six times less on graphene than on mica. Our results indicate that graphene on mica is structurally different than graphene on SiO_2 and have different impurity doping characteristics. Both of these observations are indications that electronic transport properties will also be different.

Keywords: Graphene, SiO_2, mica, Raman, AFM, LFM.

ATOMİK BOYUTTA PÜRÜZSÜZ YÜZEYLERDE GRAFEN ÖRNEKLERİNİN HAZIRLANMASI VE KARAKTERİZASYONU

Serhat YANIK

Yüksek Lisans Tezi – Fizik
Temmuz 2011

Tez Yöneticisi: Yrd. Doç. Dr. Mehmet Burak YILMAZ

ÖZ

Grafen, karbon atomlarının bal peteği yapısı şeklinde (düzgün altıgenlerden oluşan kristal yapı) örgülenmiş, tek atom kalınlığındaki katman olarak bilinir. Son dönemdeki deneysel gelişmeler mikro-mekanik ayırma yada katmanlara ayırma ve epitaksiyel büyütme yöntemleri kullanılarak tek veya çok katmanlı grafen örneklerinin hazırlanabilmesine olanak vermiştir. Mikro-mekanik ayırma yöntemi SiO_2/Si yüzeyleri üzerinde gerçekleştirilirken, epitaksiyel büyütme işlemi SiC ve bazı metal yüzeylerinde yapılmıştır. Bu gelişmeler sonucunda grafenle ilgili deneysel ve teorik araştırmalarda önemli bir artış olmuştur. Grafende, iletkenlik ve valans bantları momentum uzayında birbirine eşdeğer olmayan iki noktada birleşmektedir. Birleşim noktasında enerji momentum bağıntısı doğrusal olup Dirac Konisi adı verilen yapıyı oluşturmaktadır. Grafene duyulan ilginin temelinde bu yapının relativistik kütlesiz fermiyonların özellikleriyle benzeşmesi yatmaktadır. Bu ilginç elektronik yapı, grafeni diğer malzemelerden ayırmakta ve yarım sayı (half-integer) kuantum Hall etkisi ve sıfırdan farklı Berry fazı gibi yeni fiziksel özelliklerin gözlemlenmesine sebebiyet vermektedir.

Bu çalışmada hem silika hem de mika yüzeyleri üzerinde peeling yöntemi ile elde edilmiş grafen örneklerinin Raman ve AFM analizlerini inceledik. Silika üzerinde yaptığımız Raman ve AFM ölçümlerinin geçmiş çalışmalarda gösterilen sonuçlarla tutarlı olduğunu gördük. Mikanın atomik olarak pürüzsüz ve çok geniş bir yüzeye sahip olması mekanik soyma yöntemi ile elde edilen grafen yüzeyinin pürüzsüz olmasını sağlıyor. Silika ve mika üzerindeki grafen örneklerinin Raman spektrumlarını kıyas ettik ve silikadakinin aksine mika üzerindeki grafenin 2D modundaki tepe pozisyonunda bir değişiklik gözlemlemedik. Raman spektrumunda tepe noktaların pozisyonlarındaki bazı değişiklikler örnek yüzeyinde veya üstünde bulunan bozukluklar ya da katkılar ile ilişkilendiriliyor. Bizim elde ettiğimiz sonuç katkılanmanın atomik olarak pürüzsüz grafenin tüm yüzeyinde düzenli olduğudur. AFM ölçümlerinde grafen örneklerinin kalınlıklarını ölçmek için kullandığımız kontak moda ek olarak mikanın kendi yüzeyine kıyasla grafenin sürtünme özelliklerini ölçebilmek için yatay kuvvet mikroskobunu da (LFM) kullandık. Grafen üzerindeki sürtünme kuvvetinin mika üzerindeki sürtünme kuvvetinden yaklaşık olarak altı kat daha az olduğunu bulduk. Sonuçlarımız mika üzerindeki grafenin yapı olarak silika üzerindeki grafenden farklı olduğunu ve farklı katkılanmalara sahip olduğunu gösteriyor. Bu gözlemlemeler elektronik taşınım özelliklerinin de farklı olabileceğini ortaya koyuyor.

Anahtar Kelimeler: Grafen, SiO_2, mika, Raman, AFM, LFM.

Dedicated to my wife Ayşe Beyza, my son Vedat, and my parents

In love and gratitude

ACKNOWLEDGEMENT

First and foremost, I express sincere appreciation to my supervisor Assist. Prof. M. Burak YILMAZ for his guidance, motivation, understanding, continuous support, enlightening experience, suggestions and comments through my thesis work. Without his faith in me I would not be able to be at this level.

I would like to thank to Assoc. Prof. Dr. Kurtuluş GÖLCÜK for his valuable comments and suggestions.

Sincere thanks are also extended to the committee members Assist. Prof. Dr. Burak ESAT for his valuable suggestions, motivations and comments.

I would like to show my gratitude to Prof. Dr. Mustafa KUMRU (The head of the department of Physics) who supported me during all my undergraduate and graduate period.

Also, I am grateful to the whole Physics department academic staff for their technical, emotional, and mental support.

At last but not least, I express my thanks and appreciation to my wife, my mother, my father, and all family members for their understanding, motivation, patience and supporting me through all these years. I owe everything in my life to them.

I want to acknowledge use of BINATAM-Bionanotechnology Center equipment whics is supported by DPT. Research was funded by Fatih University grant P50011003.

TABLE OF CONTENTS

LIST OF FIGURES

LIST OF ABBREVIATIONS

AFM	: Atomic Force Microscopy
ARPES	: Angle Resolved Photoemission Spectroscopy
DFM	: Dynamic Force Mode
LFM	: Lateral Force Microscopy
nN	: Nano Newton
PMMA	: Polymethyl methacrylate
pN	: Pico Newton
PSPD	: Position Sensitive Photodetector
QHE	: Quantum Hall Effect
SEM	: Scanning Electron Microscope
SiO_2	: Silica
SLG	: Single Layer Graphene
STM	: Scanning Tunneling Microscope
UHV	: Ultra High Vacuum
μARPES	: Micro-Angle Resolved Photoemission Spectroscopy

CHAPTER 1

INTRODUCTION

It can be clearly said that the discovery of C_{60} molecule which consists of sixty carbon atoms arranged in a football shape in 1985 has brought on nanoscience to be involved in our life. After this development, in 1991, finding the carbon nanotubes launched the process of nanotechnology. Recently, this kind of discoveries have showed that carbon based structures will play a major role in the scientific progress.

Materials consisting of carbon atoms show very different physical and chemical properties depending on the binding geometry of carbon atoms. This versatility of chemical states is due to the presence of six electrons in the carbon atom. During a binding process, the absence of any effect of the first two electrons of the carbon atom provides carbon to compose different structures. These features make the carbon unopposed candidate for scientific research all around the world. Carbon atoms show three different types of bonding with each other (Fig. 1.1). These types are denoted as sp, sp^2, and sp^3 depending on the electrons that take place in binding. These designations also represent the bond geometry. In sp bonding, carbon atoms form a linear geometry with each other and each atom has two bonds as in acetylene molecule (C_2H_2). In sp^2 bonding, carbon atoms form a triangular geometry and each atom has three bonds as in graphite or graphene. In sp^3 bonding, carbon atoms are arranged in pyramidial configuration and make four bonds with each other. A well known example to such bonding is the diamond crystal.

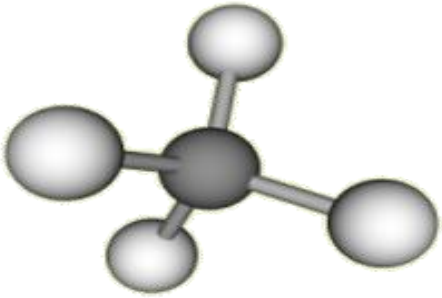

sp^3

Pyramid

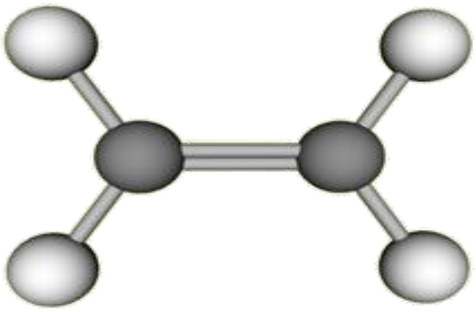

sp^2

Triangle

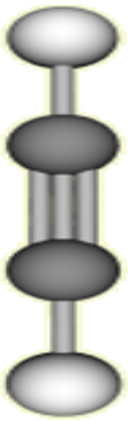

sp

Linear

Figure 1.1 The bond shapes of carbon atoms.

Graphene is the name given to a flat monolayer of carbon atoms aranged in a honeycomb lattice (Fig. 1.2). It can be seen as the building block of all other sp^2 carbon allotropes such as graphite, fullerenes, and carbon nanotubes [8]. Graphene is the first truly two-dimensional crystalline material. It can be wrapped up into 0D fullerenes, rolled into 1D single-walled carbon nanotubes, and stacked into 3D graphite. It is the thinnest material in the universe and the strongest ever measured [8]. The carbon-carbon

bond length in graphene is nearly 0.142 nm and the van der Waals diameter of one carbon atom is approximately 0.34 nm [9].

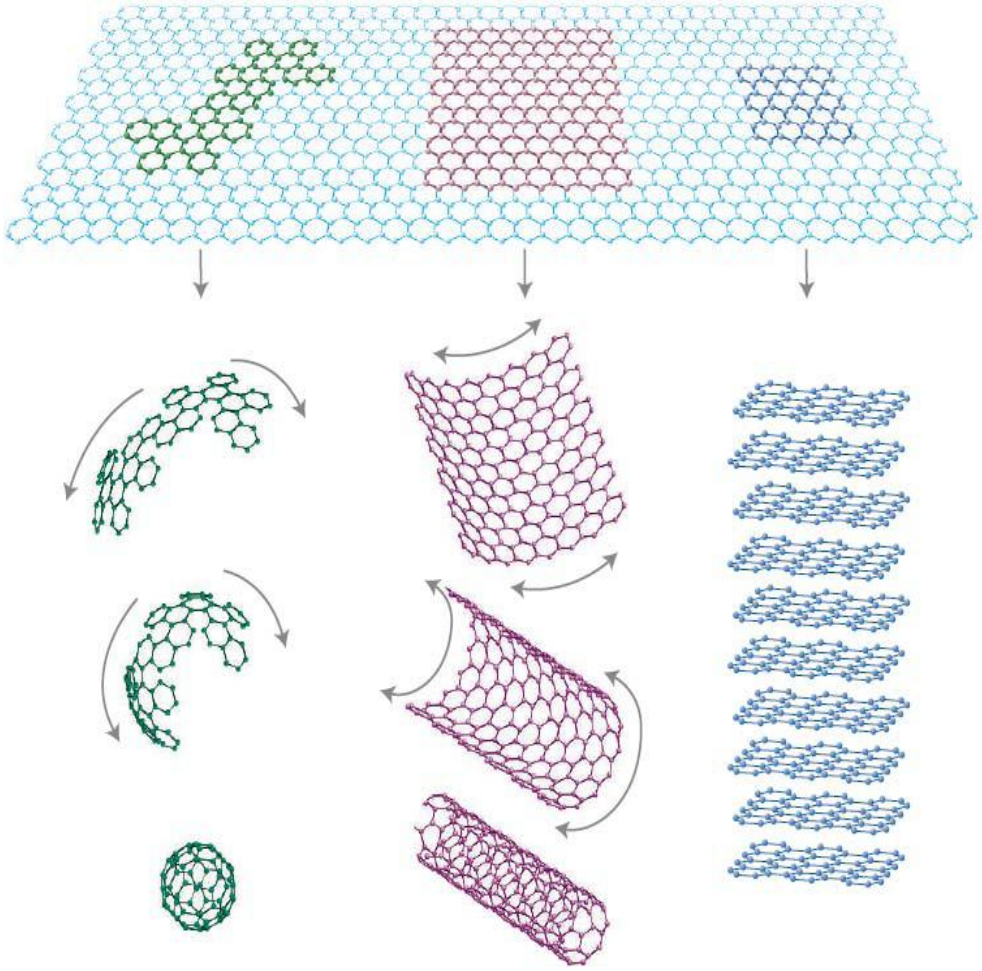

Figure 1.2 Graphitic materials transformed from graphene, including 0D fullerenes, 1D nanotubes and 3D graphite [8].

Formerly, single layer of graphite was believed to be unstable with respect to the formation of curved structures such as soot, fullerenes, and nanotubes. But in 2004, Andre Geim and Konstantin Novoselov discovered free standing graphene unexpectedly [10]. The following experiments showed that indeed the charge carriers of graphene were massless Dirac fermions [6,7]. Subsequent research lead to the discoveries of new physical phenemona such as massless excitations, anamolous quantum Hall effect, Klein tunneling, and etc. [8]. Moreover, graphene displays a relation to the particle physics.In addition, excellent crystal quality of graphene lead to the observation of extraordinary properties, such as ballistic transport, high electron mobility, and high tensile strength [8]. Ballistic transport means that the charge carriers in graphene can travel through many interatomic distances without scattering [5]. This is due to the

conjugated π orbital system which allows electrons to travel above and below the plane of carbon atoms with minimal scattering. This minimal scattering and strong delocalization features make graphene a good conductor and material of high promise for technological applications.

Prevalently, graphene samples are fabricated in two ways. These are exfoliation and epitaxial growth method. In exfoliation method, graphene samples are produced by micromechanical cleavage with a scotch tape and transferred onto Si wafers with 300 nm thick SiO_2 overlayer [5]. Using this method one-atom thick graphene specimens can be easily detected under an optical microscope [11]. Figure 1.3 shows two such graphene samples prepared as part of this thesis work. The triangular structure at the center in Fig. 1.3a is a single atom thick graphene whereas the sample shown in Fig. 1.3b has regions of differing thickness as can be seen distinguished using the different contrast of each region.

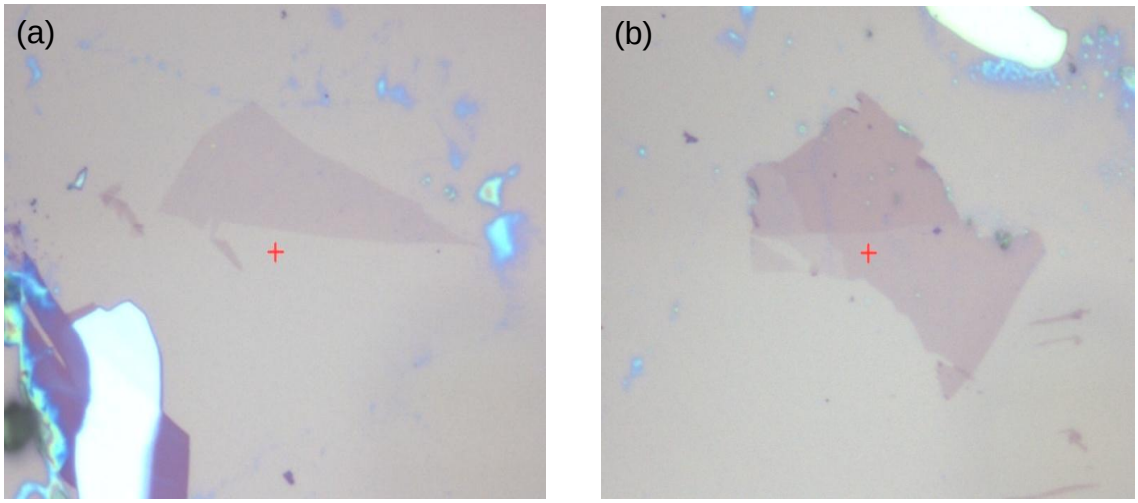

Figure 1.3 (a) Single layer and (b) multilayer graphene flakes.

Another method is to produce single or multi-layer graphene using chemical vapor deposition of hydrocarbons on metal surfaces or thermal decomposition on SiC [12,13]. However, it is observed that some crystal defects and multi-crystal domains have commonly come into existence in these samples. Due to their conductive substrates electrical measurements could not be done and the strong electronic interaction between the graphene and the metal substrate affects the band structure of the samples [13]. In order to realize anticipated electronic applications of graphene, it is inevitable to

fabricate graphene using epitaxial methods and and intensive research efforts is focused in this direction.

The optical microscopy plays a major role in obtaining graphene samples produced by exfoliation method because graphene flakes can be easily identified among hundreds of graphite particles. Nonetheless, to better understand the properties of these flakes scientists have used techniques such as atomic force microscopy (AFM), scanning electron microscopy (SEM), and scanninc tunneling microscopy (STM) methods [5,6,14,15]. The distance between single layer graphene and SiO_2 substrate is measured to be 4.2 Å with AFM under ultra high vacuum (UHV) conditions whereas the same distance is found to be about 1 nm in ambient conditions [15]. The former result is very close to the graphite interlayer distance of 3.4 Å. The latter discrepancy is attributed to the presence of contaminants (most probably water) on or underneath the graphene layer [15].

Scanning tunneling microscopy (STM) measurements demystified an important point about graphene. Despite being almost completely defect free (see Fig. 1.4a) large area scans of the sample surface showed that graphene layers on SiO_2 are in fact not perfectly flat but rather have a roughness of about 0.5 nm close to that of the substrate [14].

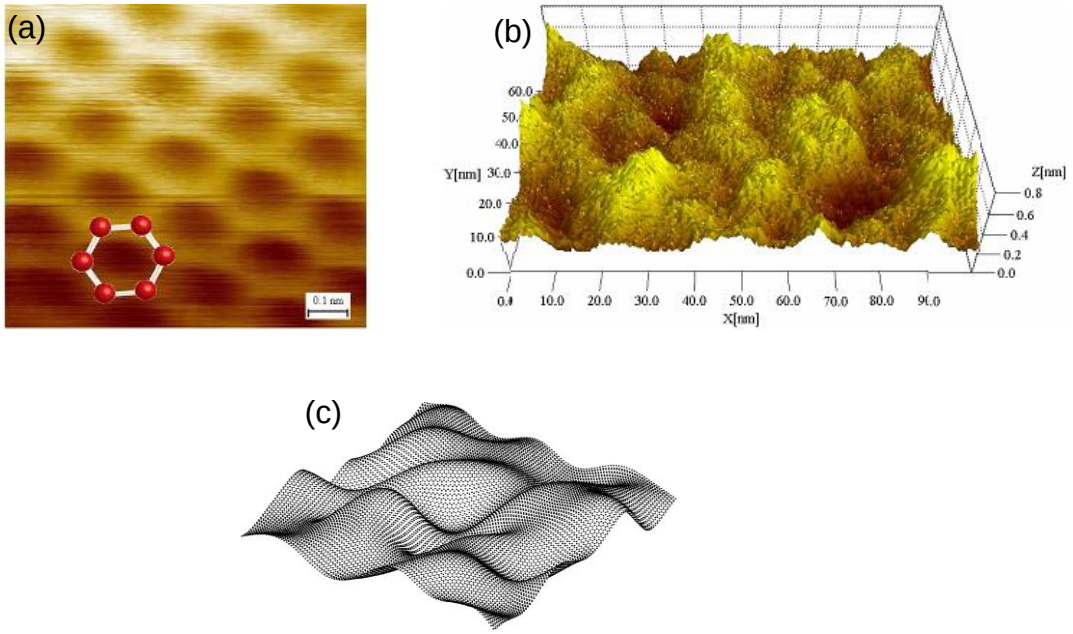

Figure 1.4 (a) The honeycomb lattice of graphene was observed using STM measurements [14]. (b) The large area scans of the surface showed that graphene surface has significant rougness [15]. (c) A model of graphene surface obtained from a computer simulation [16].

It has been shown that Raman spectroscopy can be used to identify the thickness of graphene samples [17]. Raman measurements taken from graphite displays two peaks labeled as G and 2D peaks (see Fig. 1.5b). 2D mode is derived from the second order phonon mode around the K point in the Brilliouin zone whereas G mode is derived from the interaction of carbon-carbon bonds [18,19,20]. During the transition from multilayer graphite to single layer graphene, it was observed that 2D mode shifts and gives more intense and symmetrical signal [14,17,21]. The reason of this raises the double resonance in the emission of 2D signal [17]. The intensity of G peak in single layer graphene is weaker than the 2D peak. For all other thicknesses G peak is stronger than the 2D peak.

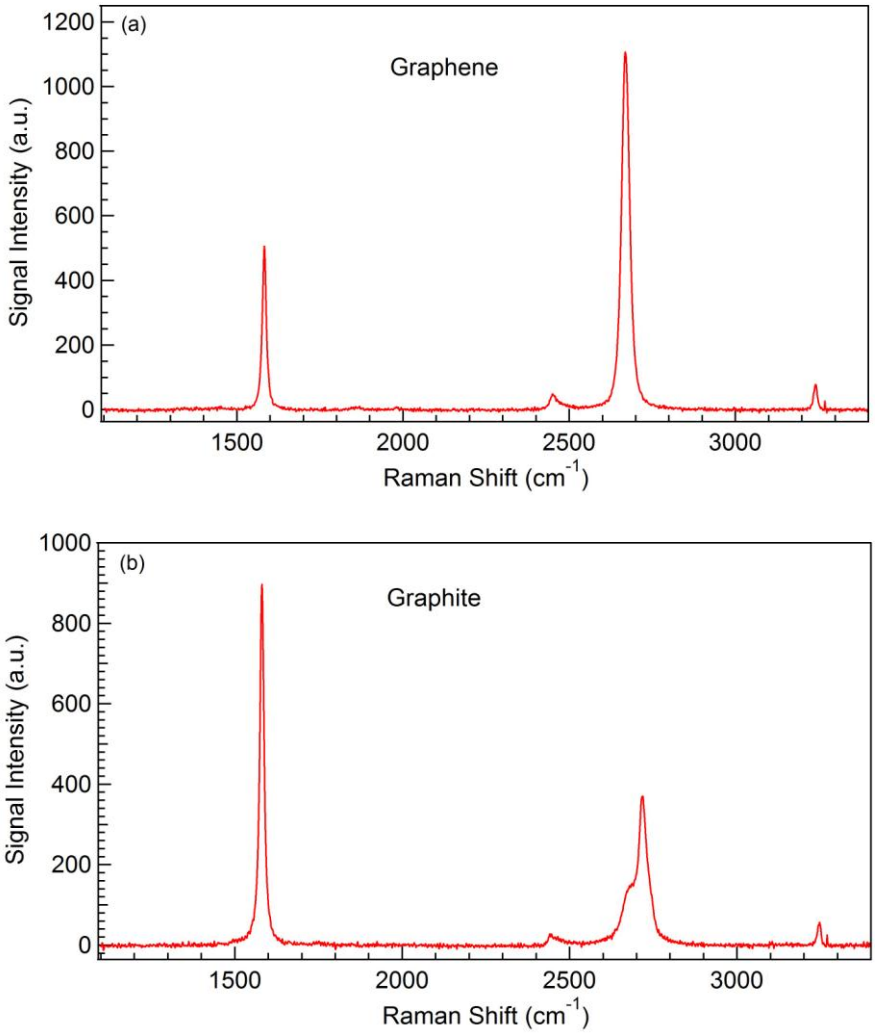

Figure 1.5 The Raman Shifts in graphene and graphite (a) Single layer graphene, (b) Graphite. G peak is at 1500 cm^{-1}, 2D peak is at 2700 cm^{-1}. The difference between graphene and graphite can be easily seen.

The investigations oriented to study electrical properties have revealed the high potential of graphene in technological applications. In graphene, the conduction and valence bands are combined at two nonequivalent points (K and K`) in the momentum space. The correlation of energy and momentum is linear at combination point and construct the structure of Dirac cone. Graphene displays an ambipolar electric field effect (Fig. 1.6a). The density of the electrons and holes can be adjusted up to $10^{13}/cm^2$ easily, and it has been observed that their mobilities can be as high as 15.000 $cm^2V^{-1}s^{-1}$ even under ambient conditions [5]. In addition, when the temperature is reduced clean suspended graphene samples can have mobility values reaching up to 200.000 $cm^2V^{-1}s^{-1}$ [22]. These results indicate that electrons can move through distance up to 0.3 µm without any scattering even at room temperature. Another indication of graphene`s excellent electronic quality is the observation of the half integer Quantum Hall Effect (QHE) at room temperature [23].

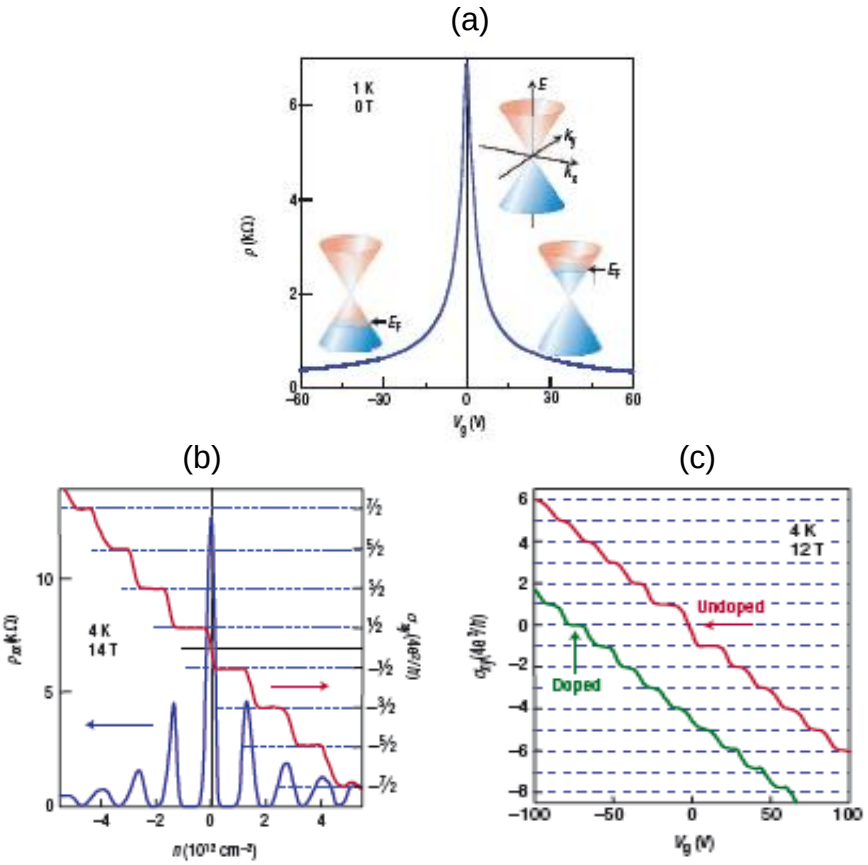

Figure 1.6 (a) The ambipolar electric field effect has been shown in single layer graphene [8]. The conic figures denote how electronic structure at K point alters by gate voltage. (b) Half integer Quantum Hall Effect in single layer graphene [24]. (c) Anomalous Quantum Hall Effect was observed in bilayer graphene.

Theoretically, properties of the electronic structure of graphene can be described using relativistic massless fermions (Dirac fermions) [25,26]. This means that, graphene appears as an invaluable material in order for probing the features of relativistic fermions. Probably Chiral Quantum Hall Effect is one of the most crucial physical effects that Dirac fermions induce (Fig. 1.6b,c) [7,24,27]. The electronic structure of graphene, can be directly observed using angle resolved photoemission spectroscopy (ARPES). These measurements have been initially done on epitaxial graphene which had been fabricated on SiC surfaces [28] and Dirac cones have been naturally observed. However, the strong interaction between the graphene on SiC and substrate and the inescapable sample doping of SiC caused Dirac point to shift approximately 0.5 eV under Fermi level. In addition STM studies of such samples indicated many crystal defects [29]. Thus, these samples does not reflect the electronic structure of high quality ones prepared by exfoliation method. However study of such samples are difficult as the sample size is very small for conventional photoemission measurements. In a recent study photoemission results were obtained using the micro-ARPES (μARPES) method. However, the results were not very satisfactory because of the low energy resolution of the instrument and the natural corrugations of the graphene samples prepared on SiO_2 (Fig. 1.7a) [30]. By improving the energy resolution, and working on suspended samples (which have less corrugation) better photoemission data is obtained more recently from exfoliated samples (Fig. 1.7b) [31].

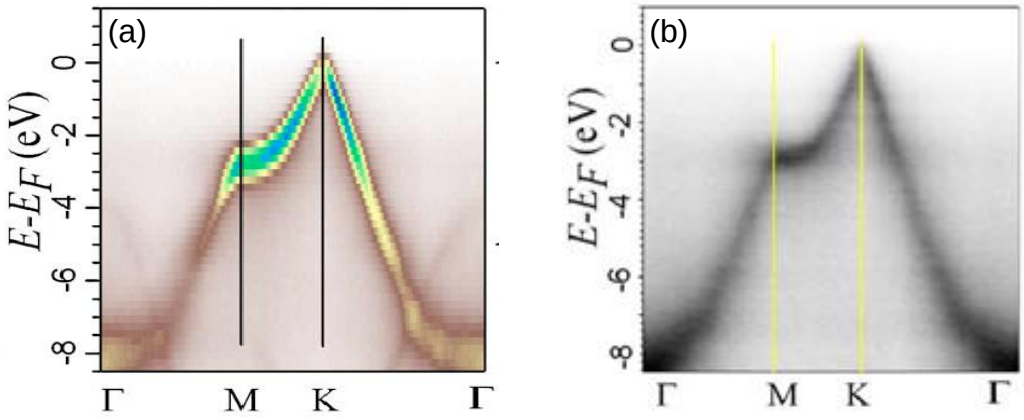

Figure 1.7 (a) The Angle Resolved Photoemission result of graphene (a) Supported by SiO_2 [30]. (b) Suspended graphene [16]. Due to reduced corrugation, the results taken from suspended graphene are better resolved. Moreover, the linear relation near Dirac point (K) can be easily observed.

Since graphene is only a single atom thick and have excellent electrical and crystal quality, it can be used as a sensitive detector. In fact F. Schedin and coworkers demonstrated that detection of single adsorption and desorption events of various gas molecules is possible using micrometer sized graphene detectors [31]. Another application is to make nanoribbons from graphene. Theoretical calculations have envisaged armchair type of nanoribbons can show semiconductive property with an energy gap depending on the width of the nanoribbon [32]. This prediction was confirmed by experiments short time ago [33]. By improving this technique, it is possible to design electrical circuits on a single atomic layer of carbon atoms (graphene film) and higher frequency devices. Small sized electronic circuits have already been fabricated on graphene [34,35]. But, it is difficult to tell these circuits show expected performance by graphene in this step. In addition to this, it will not be wrong to expect graphene used applications to enter our daily life and construct future technologies at near future.

In this dissertation, we worked on both silica and mica substrates to obtain SLG samples. Since, graphene samples on silica are now to have a finite roughness whereas graphene samples on mica are atomically flat, these two specimens are expected to have different characteristics. We aimed to study these differences using Raman, AFM and LFM techniques. Initially, we prepared graphene specimens on both silica and mica substrates and then scanned the surface of these wafers under an optical microscope to determine the location of the graphene flakes of interest. Subsequently, we performed Raman measurements to confirm the thickness of the graphene flakes. The single layer graphene samples on silica wafer appears darker than the substrate; so it is very easy to observe SLG under an optical microscope; but on mica substrate it is difficult to see a SLG under the optical microscope. As a result of this, we used Raman Mapping technique to obtain high contrast images of graphene flakes on mica substrates. Then, we operated Atomic Force Microscopy (AFM) in contact mode to measure an average thickness of the SLG. We have measured that the thickness of SLG on silica substrate was approximately 1 nm. For mica substrate the result was 0.35 nm which is consistent with the interlayer spacing of graphite. In addition to this, we obtained the frictional forces on both graphene surface and substrates to make a comparison between them. After the measurement, we have determined that the frictional force on SLG exfoliated on silica wafer was approximately 7 times less than that of silica. On the other hand, we

have found the frictional force on SLG exfoliated on mica is nearly 6 times less than that of mica. Further investigation of the Raman spectra indicated that unlike SLG on silica, the 2D mode peak position of the SLG samples does not shift for mica samples. This result, along with the 0.35 nm sample thickness lead us to think that impurity doping effects for SLG on mica is less significant than SLG on silica. We believe that this might lead to higher electrical performance of SLG on atomically smooth substrates which is the topic of another work.

CHAPTER 2

MATERIALS AND METHODS

2.1 CHARACTERIZATION TECHNIQUES

In this study, we prepared graphene samples using the exfoliation method which is explained in Section 2.2. In order to identify the samples, we used optical microscopy. Moreover, we used Raman Spectroscopy and Atomic Force Microscopy (AFM) to characterize the samples. We used optical microscopy to find the position of graphene flakes by taking advantage of interference effect of light with the substrate. Then, we measured the Raman spectrum of the flake to determine its thickness. In addition to Raman measurement we used AFM to investigate the topography of the flakes. We also studied the frictional properties of single layer graphene compared to the substrate using Lateral Force Mode (LFM) of AFM. All measurements were done under ambient conditions. In general, in addition to the Raman and AFM measurements, Scanning Electron Microscopy (SEM) and Scanning Tunneling Microscopy (STM) are used to characterize graphene samples. SEM and STM enable us to obtain the morphology of graphene samples with a high resolution. So the results of the measurements of AFM, SEM, STM, LFM, and Raman Microscopy can put forth a satisfactory understanding for consideration about graphene material when its intriguing properties are bethought.

2.2 SYNTHESIS OF GRAPHENE

There are many methods that are used to fabricate single layer (SLG) or multi-layer graphene specimens. In order to produce a SLG sample with a high quality crystal structure, the most common method is the micromechanical cleavage technique. Micromechanical cleavage is also called the exfoliation method. Other common methods can be listed as epitaxial growth on SiC or metal substrates, graphite oxide reduction, pyrolysis of sodium ethoxide, and so on. In our work, we produce our graphene samples by using the exfoliation technique. This process enabled us to obtain high quality SLG samples quickly and practically. Some of these techniques are briefly described below for reference. Epiataxial growth of graphene on SiC is one of the early methods for obtaining large area samples. The method involves sublimation of the Silicon layer at high temperetaures and formation of the honeycomb structure by the carbon overlayer that is left behind. The method requires ultra high vacuum chambers and the recipe must be precise to avoid multilayer growth. Neverthless, this method proved very useful for early investigation of the properties of graphene using techniques such as (ARPES) that require relatively large area samples. For example, the electronic band structure, weak anti-localization, and mobility properties has been studied using samples obtained by this method. One major disadvantage, however, is the quality of the samples obtained via epitaxial growth on SiC. In addition, the strong coupling of the sample with the substrate can significantly change or certain intrinsic properties of the graphene.

Epitaxial growth on metal substrates is another technique that requires in-situ measurements as epitaxial growth on SiC. In this technique, generally iridium rods are used and graphene films are grown on it. Advantages of this method are for example, Dirac cones are more visible and the samples are larger as mentioned in previous method. On the other hand, the graphene samples are not flat on iridium. There are some ripples on the surface of graphene fabricated by epitaxial growth. In addition to these the bond between the iridium rod and graphene is very weak. Moreover, in this method, employed metal is not only limited with iridium. Ruthenium was also previously used but; it has not provided better quality samples. When ruthenium rod is used for growing graphene, it has been observed that electronic properties of graphene

was affected. In addition, when ruthenium is used as the substrate , the thickness of the graphene is not uniform whereas it is uniform on iridium rods.

Graphite oxide reduction method is relatively difficult and takes a long time to produce graphene (it may take as long as a week to obtain the end product). Historically, it was one of the first techniques to synthesize graphene flakes. In this technique, some chemical processes are necessary and take too much times. In this method, graphite powder is placed in a harsh oxidation enviroment as described by the Hummer`s method [36]. After annealing and purification procedures, graphite oxide is dispersed in deionized water. It is kept under vacuum conditions for two days and compressed into a pellet and annealed again. Consequently, the quality of graphene produced by this method is lower than exfoliation method.

Pyrolysis of sodium ethoxide method becomes an alternative way for producing graphene in quantities reaching to one gram in mass. This technique consists of reduction of ethanol by sodium metal and a pyrolysis process of ethoxide. After these steps water is used to eliminate the sodium salts [37].

In this work, we used the micromechanical exfoliation method to obtain graphene samples (Fig. 2.1). In this method, thin graphite flakes are placed on a scotch tape and further thinned using multiple folding and unfolding of the scotch tape. At the end, most of the surface of the scotch tape is covered by graphite. Then, this tape is stuck on the wafer where we want to deposit our graphene flakes. For the experiments involving graphene on SiO_2 we used a highly doped silicon wafer (EDS Wafer, LLC) with a thermally grown 300 nm oxide layer. This thickness make it easier to see graphene flakes under the optical microscope due to finite transmission of graphene and an interference effect [11]. The SiO_2/Si wafers were first cleaned using a piranha solution in an ultrasound bath for half an hour at room temperature and then thoroughly washed using distilled water and ultrapure methanol. Piranha solution is prepared by mixing 95-98% H_2SO_4 with 30% H_2O_2 at a 3:1 ratio by slowly adding acid to H_2O_2 in an ice bath to avoid violent exothermal reactions. For the experiments involving mica substrates V5 grade mica (SPI) were used. These mica pieces were cut into 2 cm x 2 cm dimensions and then graphite coated scotch tapes were placed on the freshly cleaved mica surfaces.

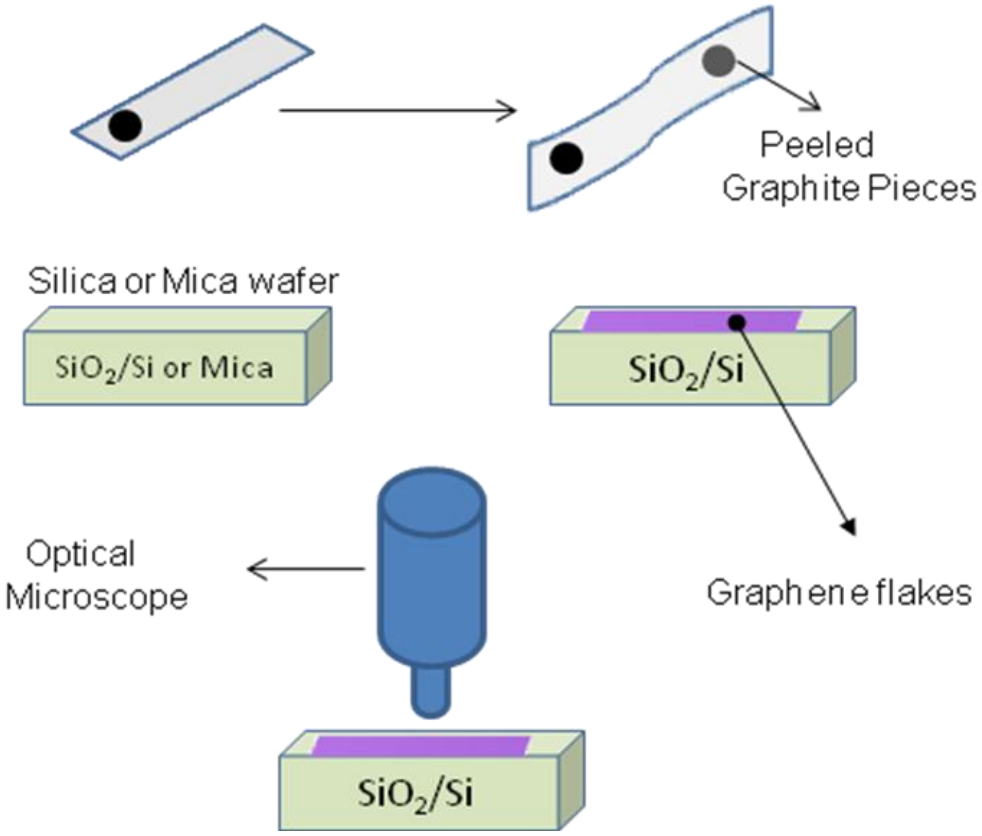

Figure 2.1 Illustration of the scotch tape method that is the most prevalent one among the other techniques in order to fabricate graphene samples.

2.3 RAMAN SPECTROSCOPY

As is known, the light consists of photons. If these photons interact with matter for example, with substances such as particles, they get absorbed, scattered or pass through the matter without any interaction. In an absorption process, when the energy of a photon corresponds to the energy difference between the ground state and the excited state of the material it is interacting with, it will be absorbed and lead the material to have a higher energy than before. On the other hand, it may also get scattered as a result of the interaction with or without losing part of its energy. The energy, scattering direction and intensity of these photons can be measured using a photodetector and analyzed to obtain information about the material interacting with the light. Such

measurements can be utilized to determine the size of particles, type of chemical bonds involved within the material and even the electronic structure of the material.

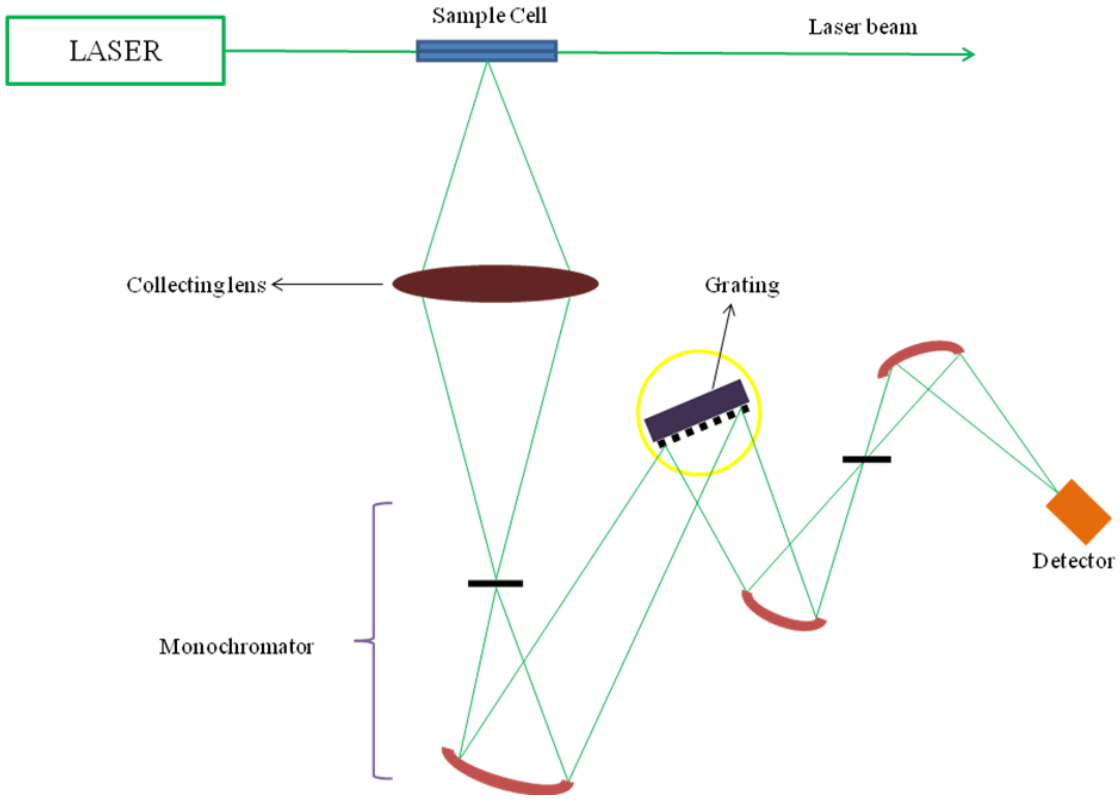

Figure 2.2 Schematic diagram of a Raman spectrometer.

Raman scattering is a technique which is used in Raman Spectroscopy to charaterize and identify the molecules. In Raman spectroscopy, a single frequency of radiation is used to irradiate the sample. This is easy to achieve with the use of modern lasers and microscopes. Raman spectroscopy involves an interaction between the molecule and the photon. In addition to the backreflected and transmitted light as is commonly observed, light can get scattered through three different processes. In the so called Rayleigh scattering process, the photon gets absorbed and excites the molecule to a higher energy state (or a virtual state) and the molecule returns back to its initial level by emitting a photon with exactly the same energy in some other direction (Fig. 2.3a). Because, energy of the incident photon is equal to the photon emitted by the molecule, this scattering is similar to the elastic scattering process of particles.

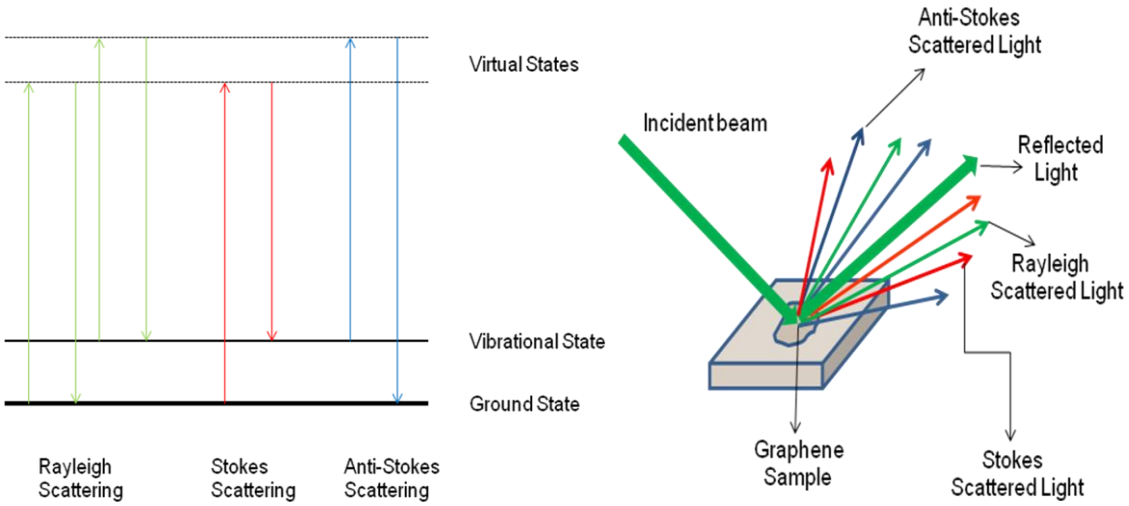

Figure 2.3 (a) General illustration of three types of scattering processes of light with matter. The dashed lines indicate the virtual energy state of the molecules according to the energy of the incident photon. (b) Diagram of a rare Raman scattering among different scattered photons.

In addition to Rayleigh scattering, there are two another types of scatterings such as Stokes and Anti-Stokes scattering. The stokes scattering is the name given to a process which takes over an inelastic scattering of a photon (Fig.2.3b). In contrast to Rayleigh scattering, molecule absorbs energy and after the vibrational excitation of the molecule, lower energy photon is released by the molecule and there remains an excess energy. As a result of this, distorted molecule starts to vibrate in an upper vibrational energy state steadily. This is also called as a Raman scattering. The stokes scattering is a much rarer case which includes only one in 10^6-10^8 of the photons scattered. Figure 2.3b illustrates this scattering as an example for a better comprehension.

The anti-stokes scattering is the inverse condition of stokes scattering in basic terms. Contrary to the stokes, molecule loses energy and after the vibrational excitation of the molecule, higher energy photon is released by the molecule. So, it takes a place in ground state or a lower vibrational energy state compared to the initial condition as mentioned in Figure 2.3a.

Generally at room temperature most molecules vibrate in the lowest vibrational energy level. Most molecules scatter from the ground state but; occasionally, some molecules are present in an excited state by the reason of thermal energy. If these molecules scatter from this excited state to the ground state, this process is called Anti-Stokes scattering. As we mentioned previously, Rayleigh scattering does not involve

any energy change. Hence, the most intense process is the Rayleigh scattering with respect to the Stokes and Anti-Stokes scattering. The second intense process is the stokes and the third one is Anti-Stokes. The scattering probability depends on the number of molecules in the ground state or excited vibrational states. It can be calculated using the Boltzmann equation:

$$\frac{N_n}{N_m} = \frac{g_n}{g_m} \exp\left(- \frac{E_n - E_m}{k_B T} \right)$$

where N_n is the number of molecules in the excited vibrational energy level n, N_m is the number of molecules in the initial vibrational energy level m, g_n and g_m are the degeneracies of the levels n and m respectively, E_n–E_m is the energy difference between the two vibrational levels, k_B is the Boltzmann's constant, and T is the temperature.

2.4 ATOMIC FORCE MICROSCOPY

Atomic Force Microscopy (AFM) was developed as a pro level of Scanning Tunneling Microscopy (STM). Because, soon after STM was invented, there was a question; " How can nonconductor surfaces be measured? ". As it is understood from the question, STM could only image conducting or semiconducting surfaces. On the other hand, AFM can operate on all kind of surfaces without regard to conducting or insulating surfaces. Glasses, polymers, seramics, nano composites, and biological samples etc. can be characterized by AFM. Accordingly, we can say the AFM was mainly developed for nonconducting surfaces. Basically, AFM is operated with a laser deflected from the cantilever and a photodetector which from we can understand the position of the laser. Figure 2.4 shows this process schematically. Theoretically, AFM measure the force between the surface and tip. Figure 2.5 shows the image of the tips by Scanning Electron Microscopy (SEM). Accordingly, to know this force accurately is the key point for proper monitoring. Namely, force is not measured directly; but calculated by measurement of the position of deflected beam.

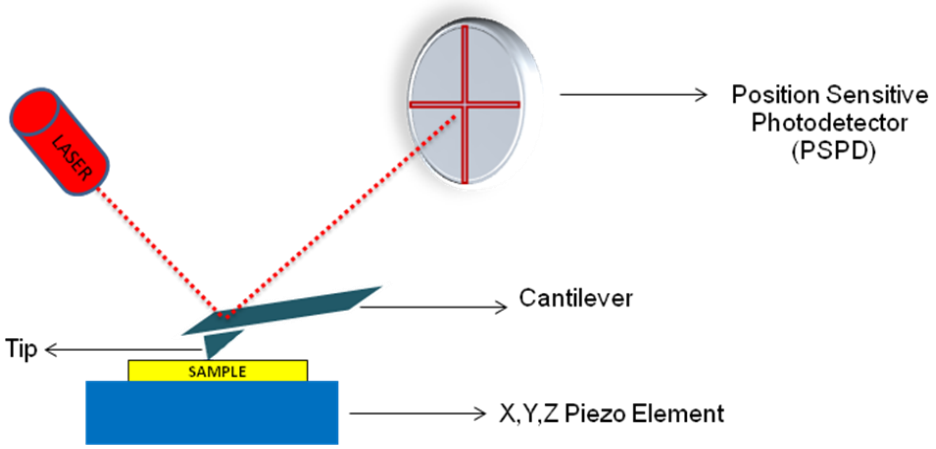

Figure 2.4 Theoretical principle of AFM, using a laser and photodetector to adjust the position.

Here, the stiffness of cantilever is also important for operations. We can explain this situation by Hooke's Law which represented in Figure 2.6.

$$F = -kz$$

In this formula, F represents the force between the tip and sample, *k* corresponds to the stiffness of the cantilever, and *z* gives the distance of bending of the tip.

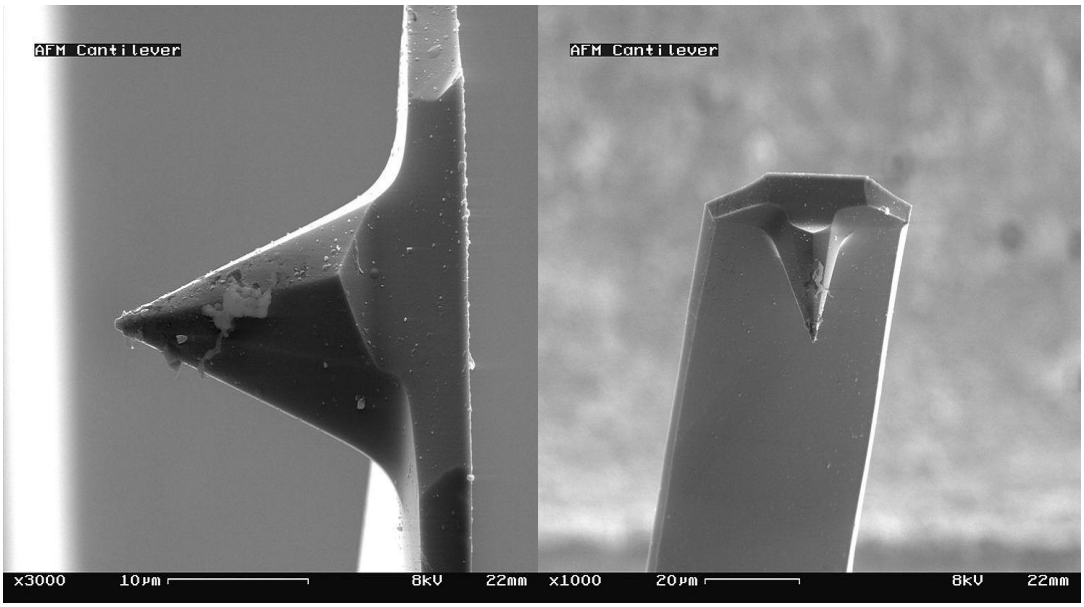

Figure 2.5 Example of SEM images of the AFM cantilevers [42].

Atomic Force Microscopy system has a large research area all over the world. So it holds a place in a great number of probe topics. What is more, when some special applications are in case of necessity it can be modified. Prevalently, AFM operates in a constant force between the tip and the sample or by moving the sample. This technique provides us to take an image but we can get more useful results by changing the modes of AFM. Recently, different type of modes started to be used for varying purposes. In this part of the thesis, these different types of mode will be introduced in turn. At first, the modes will be defined and then some examples about their capability for technological applications that used to characterize the materials or probe their physical, structural, electrical, magnetic, and frictional properties wiil be given.

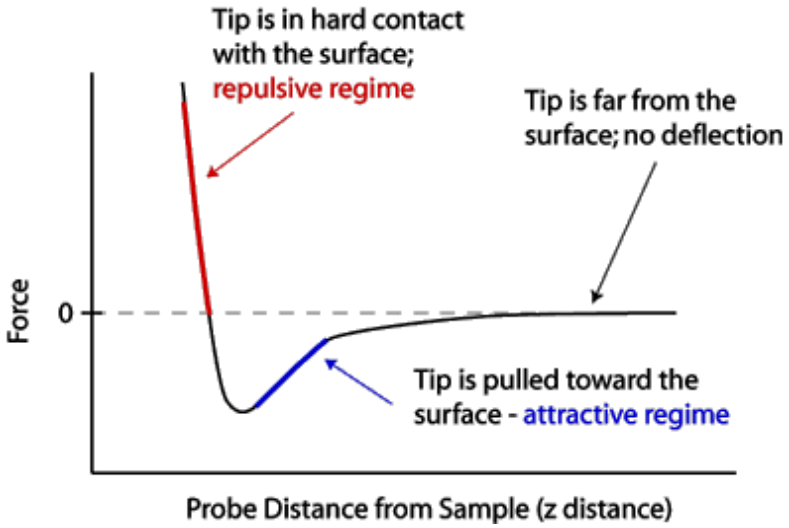

Figure 2.6 When the tip is brought into proximity of a sample surface forces between the tip and the sample lead to a deflection of the cantilever according to Hooke's law.

2.2.1 Contact Mode

Contact mode is the most common type among the other modes. It has a large usage area. In this mode, the tip is scanned across the surface by touching. To visualize this method in our minds, the tip can be thought as a needle which works in recording devices. In contact mode the force between the tip and sample is kept constant by preserving a constant deflection. Contact mode can also be operated under fluids with similar high resolution to that in air. Generally, the spring constant of the cantilevers that used in contact mode is in the range of 0.01 to 10 N/m

2.2.2 Non-contact Mode

In non-contact mode the tip is never in touch with the substrate. So, it differs from the contact mode with this property. Non-contact mode is most suitable for soft materials or samples. In addition to this, the force between the sample and the tip is lower than contact mode because the tip is moved on the surface without any touching. Approximately this force has a value of 1 pN. With this method, the data from the sample or topography images are extracted using the variance of resonance frequency or the amplitude of the cantilever.

2.2.3 Tapping Mode

In addition to these modes, there is another type of mode that is called tapping mode. In order to overcome the limitations of contact mode imaging as mentioned above, the intermittent, or tapping, mode of imaging was developed [43,44]. Commonly, it is also called Dynamic Force Mode (DFM). In this mode, a stiff cantilever oscillates on the surface at a distance that is closer than in non-contact mode. For that reason, while the tip oscillates, it extends into the repulsive field and touches or taps the surface of the sample periodically. In order to prevent the tip not to stick on surface, very stiff cantilevers are typically used. The advantageous part of the tapping mode is getting high lateral resolution on soft samples. In this thesis, we have also observe the lateral force on graphene surfaces. Hence, some brief information about the Lateral Force Mode will be given.

2.2.4 Lateral or Frictional Force Mode

In frictional mode, as the tip is scanned across a surface the forces exerted on the tip in the x direction or lateral direction are recorded at the same time. While working with lateral mode, we have to take some important points into account for extracting quantitative datas from measurements. These are, for example, normal force applied by the tip, the lateral spring constant of the cantilever, geometry of the tip apex, and the sensitivity of the optical lever to the torsional bending of the lever arm that holds the tip at the end of it [45,46].

CHAPTER 3

RESULTS AND DISCUSSION

3.1 OPTICAL MICROSCOPY

Graphene samples prepared on SiO_2 and mica surfaces are first investigated under optical microscope. During this stage, we have scanned the surface of the substrate to find graphene flakes with appropriate size and thicknesses among the thousands of bigger and thicker graphite particles. Although not a quantitative technique, optical microscopy can be used to approximately determine the thickness of the sample from the contrast between the substrate and the flakes.

In the case of the SiO_2 substrate, graphene flakes appear slightly darker when compared to the wafer surface with increasing contrast as we move to thicker and thicker flakes (see Fig. 3.1). Among the different thicknesses, single layer graphene can be barely distinguised in comparison to the background. On the other hand, bilayer and trilayer graphene has a darker color compared to the single layer and is fairly easy to see under the optical microscope. Beyond a certain thickness, the graphite pieces no longer transmit the light and the substrate is no longer visible. Since graphite is reflective, such pieces appear bright on the surface. On Fig. 3.1, the irregularly shaped, smeared out stains on the left are the scotch tape residue that is left behind during the exfoliation process. In this particular image, the trilayer graphene piece is convenient for Raman and AFM studies as it is fairly large and free from contaminants. However, the single and bilayer pieces are not very good for this purpose because they are small and right next to a thick graphite flake which may hamper experimental study of the sample. During our research we have prepared many graphene specimens and picked the most proper samples for the specific experiment.

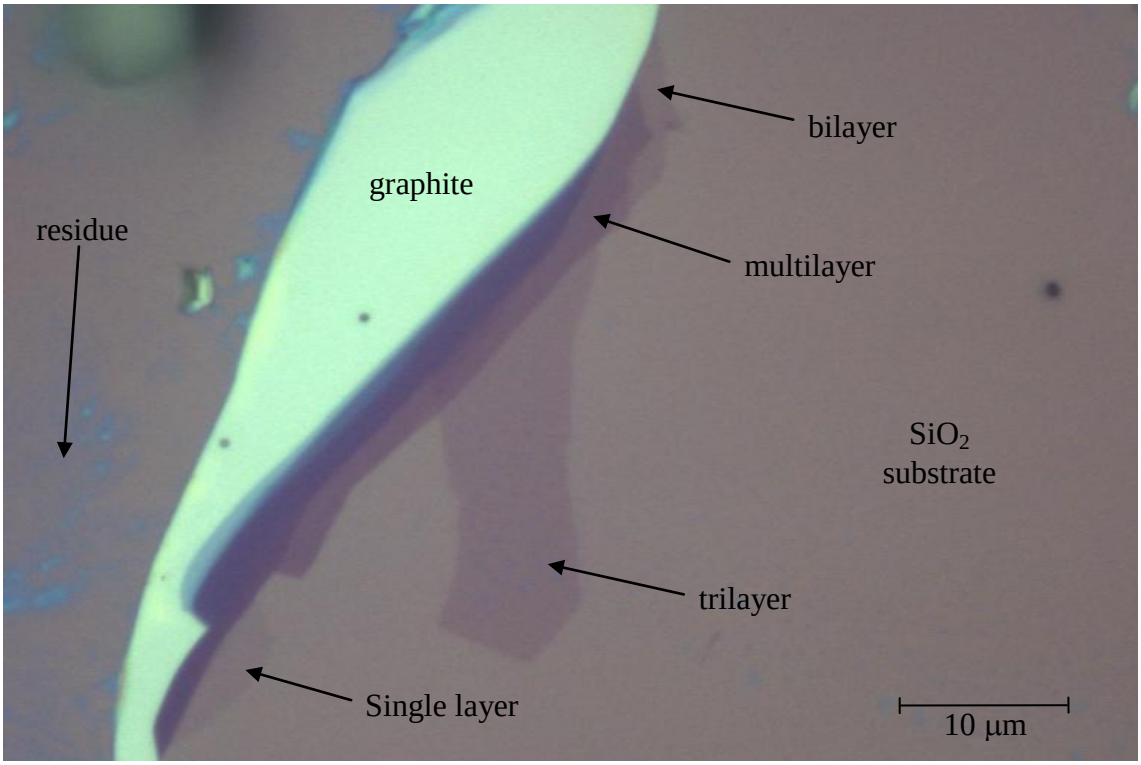

Figure 3.1 Optical image of a graphite piece on SiO_2 substrate containing regions with different thicknesses with 100x objective. The right side of the image is the SiO_2 substrate and the bright piece crossing the middle of the image is graphite. A single layer and trilayer graphene attached to the graphite can be seen easily on the image. The irregularly shaped bluish stains on left side of the image are the scotch tape residue.

On mica substrates, the optical microscopy is also useful in identifying graphene samples suitable for experimental investigation. Figure 3.2 depicts two images obtained from a mica substrate. In the case of mica, both graphene and graphite pieces appear brighter compared to the mica substrate. In Fig. 3.2a, a graphite piece with various thicknesses appear at the center of the picture. There are no few layer graphene on this piece but fairly thin graphene region appears on the right side of the sample. An approximately 10 mm wide single layer graphene can be seen at the center of Fig. 3.2b. Although brighter than the mica substrate, single layer graphene is hardly visible even in this image processed picture. In our experience, we were only able to recognize single layer graphene samples with 100x objective.

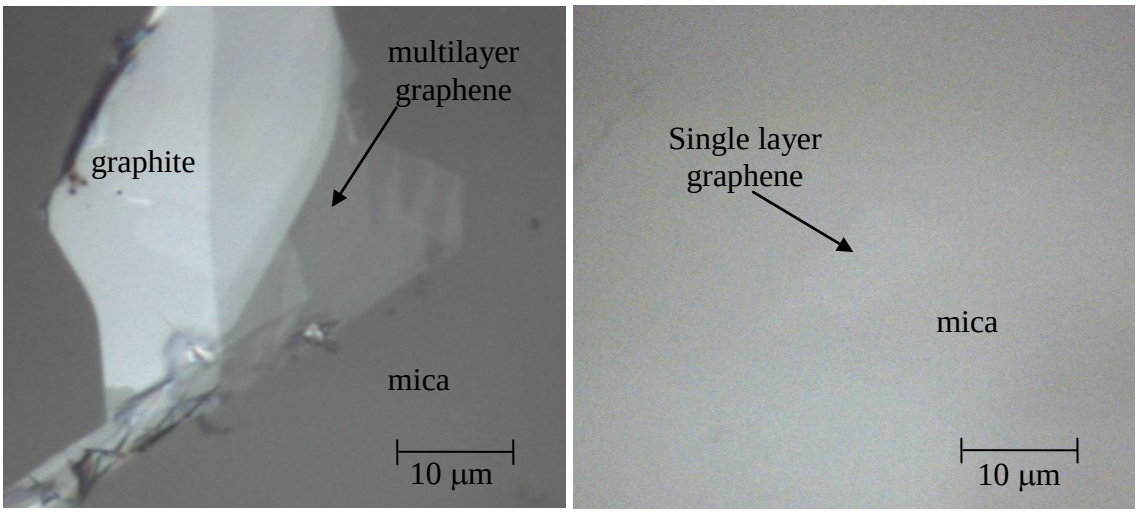

Figure 3.2 (a) Optical image of a graphite piece on mica substrate containing regions with different thicknesses with 100x objective. (b) Optical image of a single layer graphene on mica with 100x objective. Both graphene and graphite appears brighter than mica.

The differences between the images from SiO_2 substrate and mica can be attributed to the physical properties of the substrates. In the case of SiO_2, the substrate is a 300 nm thick layer on Si crystal. The Si crystal is reflective and a significant amount of light gets reflected from SiO_2/Si interface and interferes with the light reflected from the SiO_2/air interface. This gives the surface its purple color. When graphene is placed on the substrate, it blocks part of this reflected light due to its finite transmittance and also the interference condition slightly changes due to additional thickness of the graphene. As a result a contrast appears between the graphene covered and bare regions. Mica, however, is transparent and the amount of reflected light from the mica surface is minimal. When graphene is placed on the mica the light reflected from the surface increases and hence appears brighter than the bare mica. As the thickness increases, light reflected from graphene increases as well at it becomes more and more brighter.

3.2. RAMAN SPECTROSCOPY AND MICROSCOPY

The easiest way to determine the thickness of few layer graphene is to measure its Raman spectrum. Figure 3.3 displays the Raman spectrum of single layer graphene and graphite on SiO_2/Si. The differences between the two figures is apparent. The G peak appearing at approximately 1550 cm^{-1} is weaker than the 2D peak appearing approximately at 2700 cm^{-1} on graphene. However, the intensities of the two peaks are reversed on graphite samples. The higher intensity of 2D peak on graphene is attributed

to the double resonance of 2D mode as mentioned earlier. In addition, the 2D peak on graphene is centered at a slightly less Raman shift and have a symmetrical shape when compared to the one from graphite samples. By noticing these two features we can easily identify single layer graphene samples both on SiO_2 and mica substrates. It is interesting to note that the intensity of the Raman peak from single layer graphene is comparable to the intensity obtained from graphite samples. One would normally expect

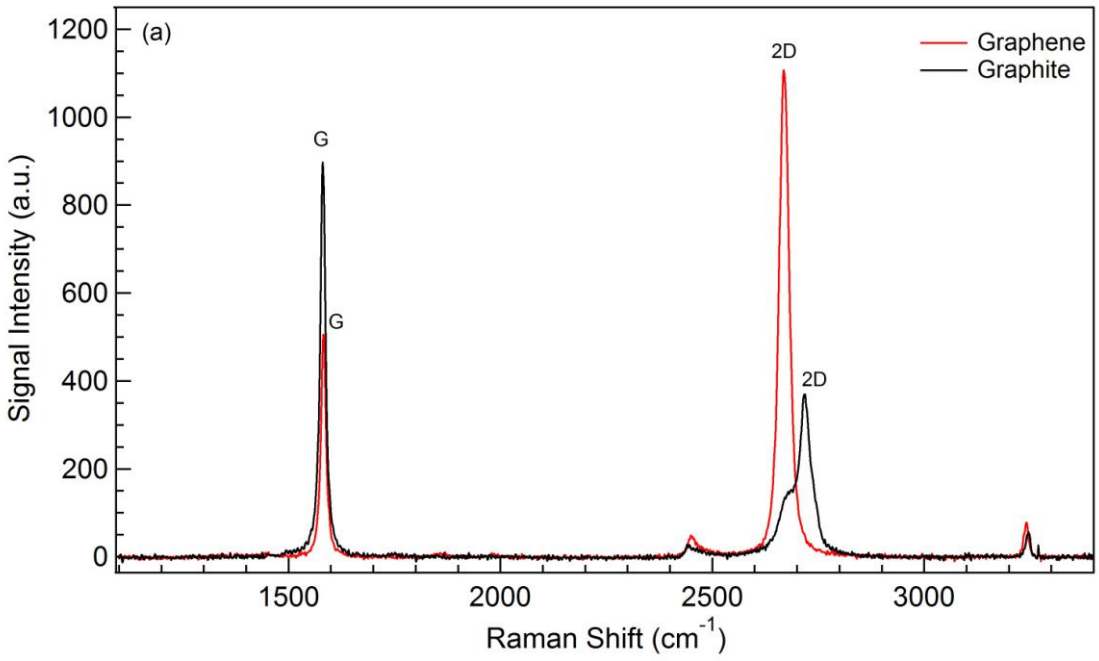

Figure 3.3 The Raman Shifts of graphene and graphite on silica substrate. G peak is at 1500 cm^{-1}, 2D peak is at 2700 cm^{-1}. The difference between graphene and graphite can be easily seen.

the signal from single atomic layer to be weaker as there is less material to interact with the exciting laser beam but thanks to the interference enhancement of the 300 nm thick SiO_2 layer graphene intensity is as strong as the graphite intensity. Another important conclusion from the Raman measurement is the high crystal quality of the graphene samples used in our experiments. The D peak of graphite and graphene at 1350 cm^{-1} appears only if the crystal has significant amount of defects. As is clear from Fig. 3.3 both the graphene and graphite samples does not show any peaks at 1350 cm^{-1} indicating that the samples are free from defects within the sensitivity level of the Raman spectrometry.

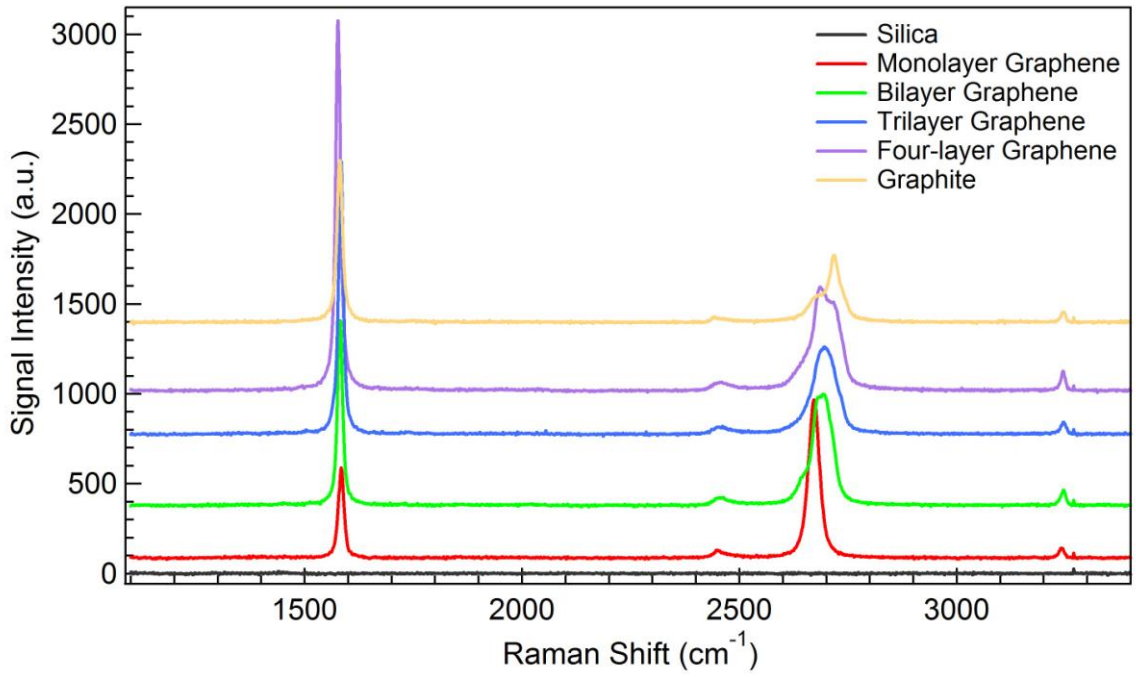

Figure 3.4 The Raman spectra of the monolayer and multilayer graphene samples on silica substrate. It is clearly seen that graphene has a different spectra rather than multilayer graphene and graphite.

Figure 3.4 displays the Raman spectra from graphene of several different thicknesses and graphite. There are two important features that can be observed in this figure. First, the G peak intensity at ~1550 cm^{-1} is increasing almost linearly as the number of graphene layers being studied increases. This is an expected behaviour because as the number of layers increases the amount of carbon atoms interacting with the light increase resulting in higher Raman intensity. However, although the number of layers on graphite is much bigger than few layer graphene, the G peak intensity is weaker. This is due to the lack of interference effect mentioned earlier in the case of graphite. Hence, relative intensities of few layer graphene may be used as a guide in determination of the thickness of the sheet. Second, the shape of the 2D peak at ~2700 cm^{-1} is changing significantly as the number of layers are changed. These shapes are characteristic of their particular thicknesses and changes are attributed to the changes in the band structure of graphene near the Dirac point. Since, these changes are also affecting the Raman cross-sections, the intensity of the 2D peak does not change significantly as the sample thickness is increased.

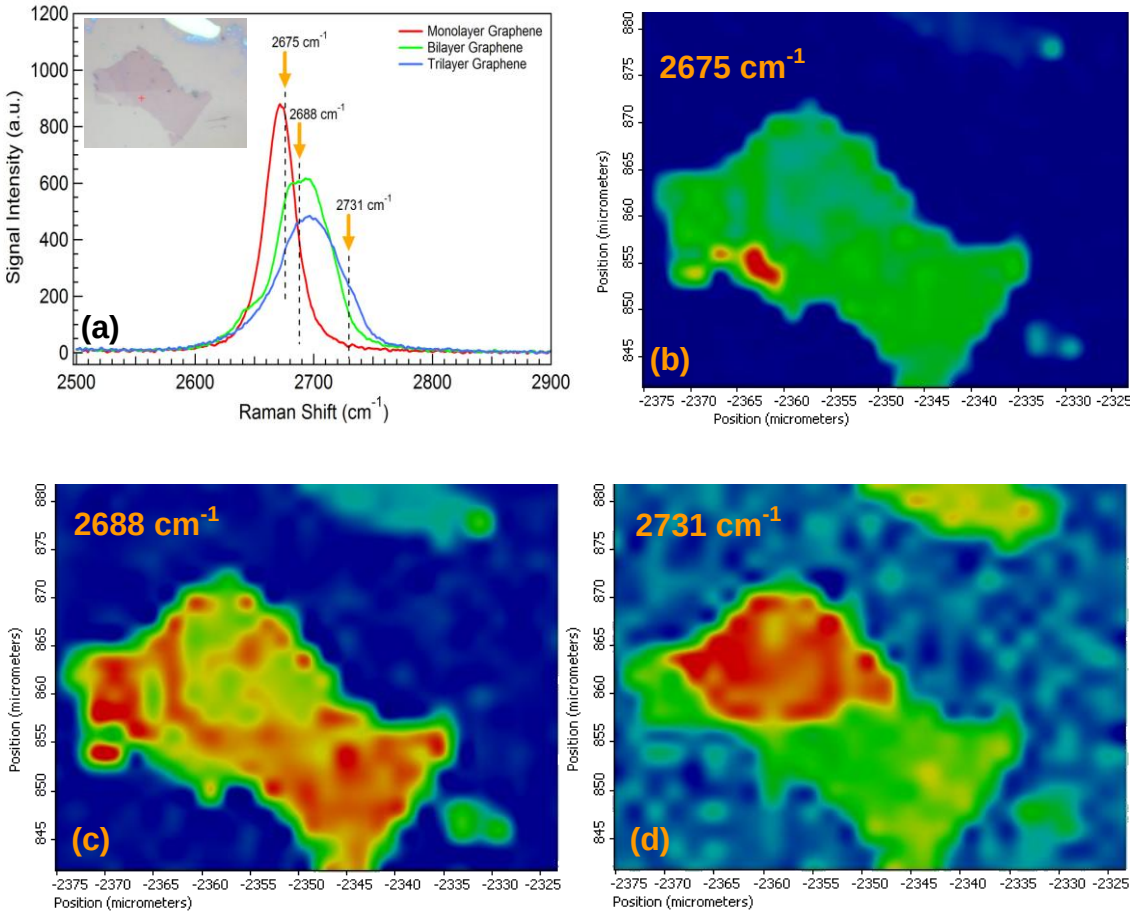

Figure 3.5 (a) Single, double, and triple layer graphene 2D peaks obtained from a single flake on SiO_2 (see Inset). (b-d) Raman Image Maps obtained from the same sample at three different Raman shifts displays the Raman intensity as a function of position.

Another investigative tool of Raman microscopy is Raman mapping. In this method, the sample is moved under the Raman microscope objective in steps to scan the sample surface and spectroscopic data is collected from each point. In that way, the spatial variations of the Raman response can be monitored. We have collected such data from a graphene sample composed of single, double and triple layer graphene. Figure 3.5a shows the 2D peak intensity obtained from these three diffrent parts of the flake. Since, each 2D peak has a different line shape and intensity, Raman images formed using intensity values at different Raman shifts can be used as a tool to distinguish layers of different thicknesses. For example, in Fig. 3.5b, the image is formed at a Raman shift of 2675 cm^{-1} which corresponds to the single layer 2D peak position. In this case, the highest intensity comes from the single layer portions of the sample. For the particular sample in Fig. 3.5b there is a small single layer piece (appearing as red) on the lower left portion of the flake. Fig. 3.5c and d are images taken at two other

Raman shifts (2688 cm^{-1} and 2731 cm^{-1}) selected such that the double layer and triple layer regions appear dominant in the image. As can also be seen from the optical image inset to Fig. 3.5a, there are two double layer regions on the upper left and lower right part of the flake and a triple layer region on the upper right portion.

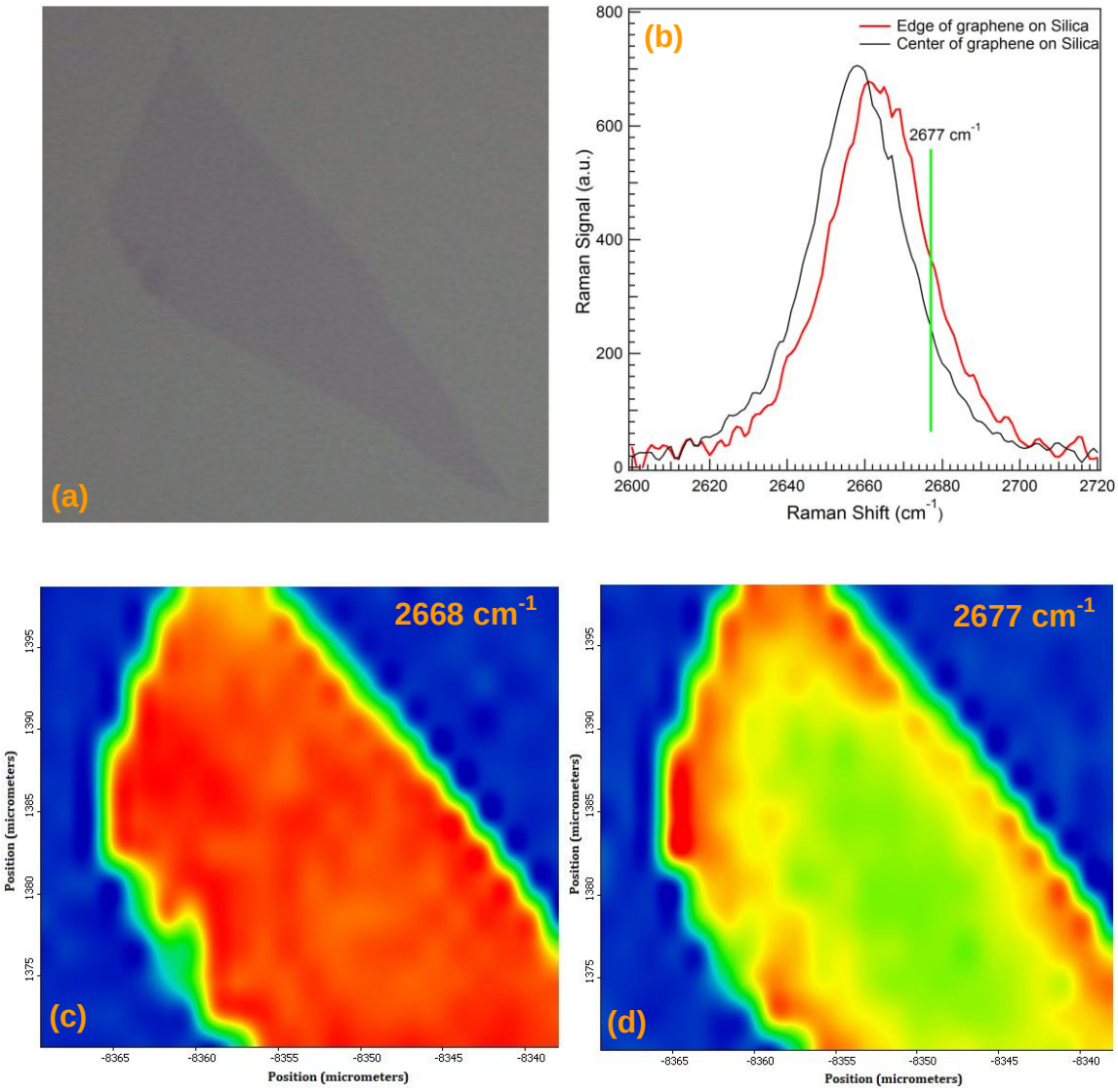

Figure 3.6 (a) Optical image of a single layer graphene on SiO_2. (b) Raman 2D-mode spectra from the side and the center of the same graphene flake. (c) Raman intensity image at a raman shift of 2668 cm^{-1}. (d) Raman intensity image at a raman shift of 2677 cm^{-1}.

In order to study the variations in the raman spectrum within a single flake, we collected Raman map data from single layer graphene piece on SiO_2. The optical image of the sample that we studied is shown in Fig. 3.6a. The sample is mostly one atom thick except for the small part on the lower left side of the sample where the flake has

folded back on the itself to form a two atom thick layer. Figure 3.6b shows the 2D-mode peaks measured from the center and near the edge of the sample. Clearly the data from the side displays an upshifted 2D-mode feature. When the raman image is composed at 2668 cm^{-1} (see Fig. 3.6c), the signal intensity from the graphene appears to be uniform all around the sample. However, a similar image at 2677 cm^{-1} appears much different. In this case the intensity at the center of the sample is weaker and appear in green and yellow tones whereas the signal from the edges of the sample is red (more intense). This confirms that the upshift of the 2D-mode in Fig. 3.6b is an edge effect of the graphene on SiO_2 because due to the upshifting of the line, the signal at 2677 cm^{-1} is consistently higher at the edge than it is at the center. It has previously been observed that 2D-mode features upshift in energy when they are hole-doped by gating the sample [47]. We believe that the shift at the edges of the sample is also due to local hole doping of the sample by contaminants such as water and oxygen and also by the substrate itself. Such contamination occurs all over the sample however, the consistent upshift around the edges indicates that adsorption of such contaminants to the graphene is more likely at the edges of the sample.

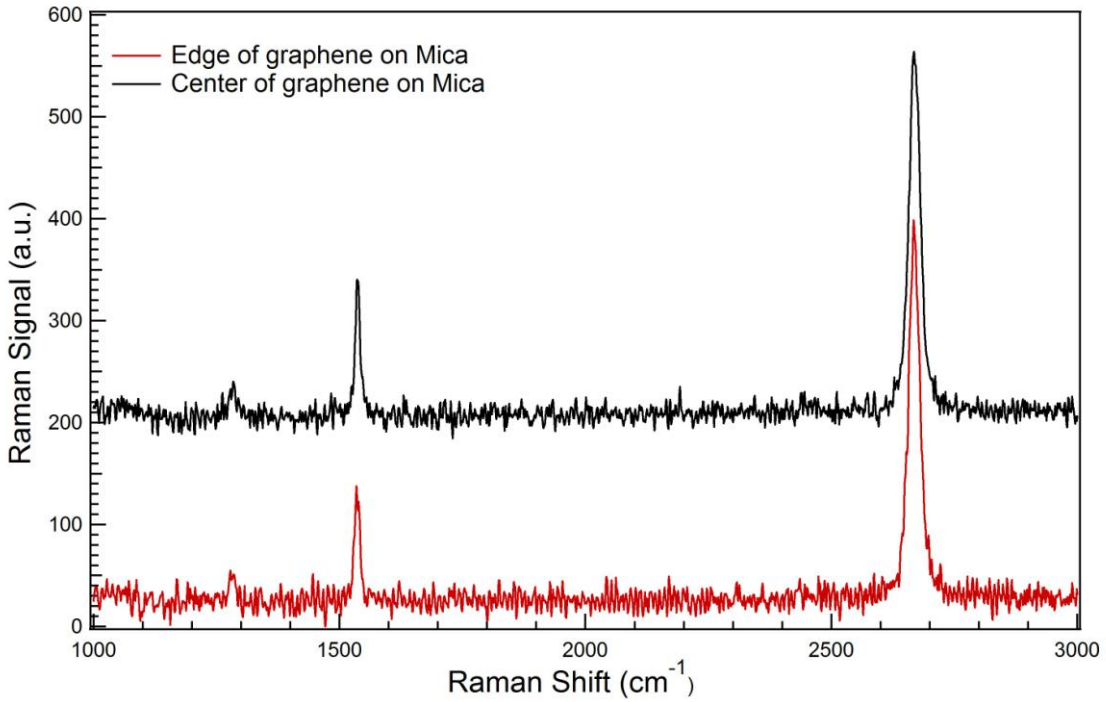

Figure 3.7 The Raman Spectra both from the edge of graphene on mica substrate and center of graphene on mica substrate.

As seen in Figure 3.7, the Raman spectrum of graphene which is deposited on the mica surface by exfoliation method is similar to that on the silica substrate. The Raman signal intensity on mica substrate is weaker than the intensity on the silica substrate because the interference enhancement observed on the 300 nm thick silica overlayer is absent in this case. Similar to the measurements from graphene on silica, we have collected data from the central and edge regions of the graphene sample on mica. The figure shows that the Raman signal from the center and the edge are equivalent to each other. To confim that this is consistent from all over the sample we have formed a Raman intensity image at 2676 cm^{-1} shift as shown in Fig. 3.8. An additional benefit of this image is that the graphene sample is better defined in comparison to the optical image where the sample is hardly visible (see Fig. 3.2b). Unlike Fig. 3.7d, where the edge signal is stronger than the central regions, the Raman signal of graphene on mica substrate in Fig. 3.8 is uniform in intensity for all positions. The fact that the Raman 2D peak has shifted by the same amount and that the peak intensity is uniform at all points is an indication that the doping of graphene is uniform on mica substrate.

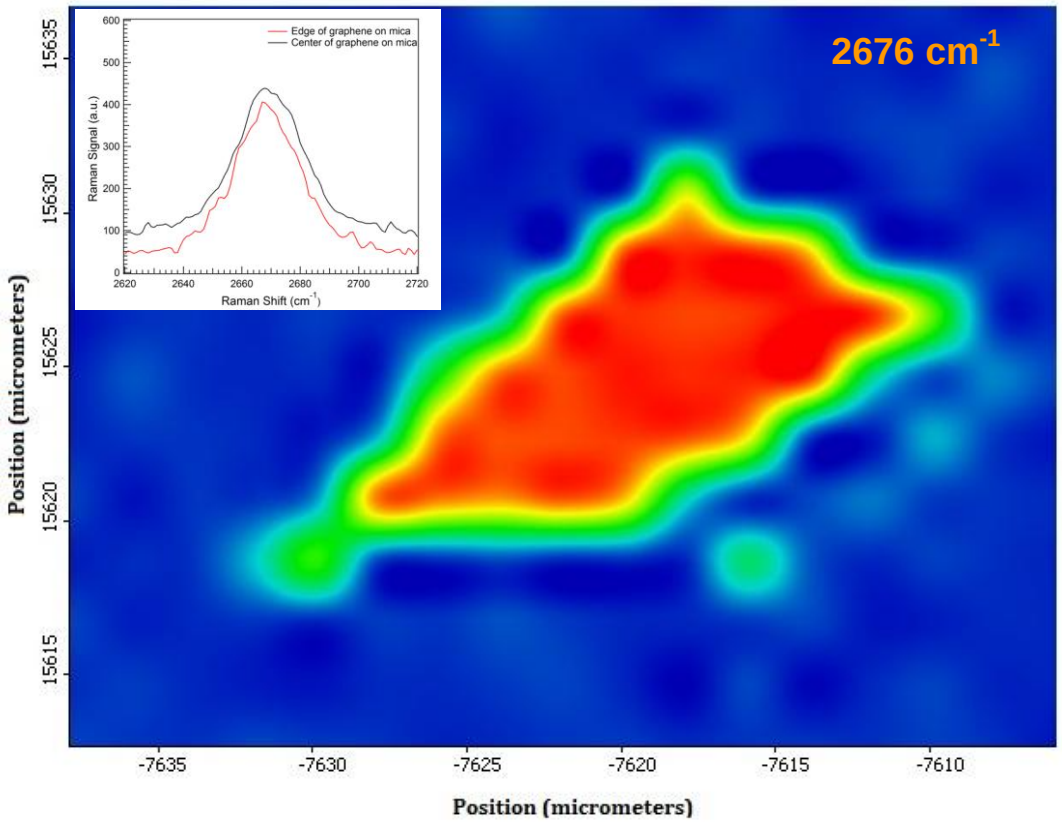

Figure 3.8 The raman image of a single layer graphene on mica substrate. Inset figure displays the Raman 2D mode from the center and the edge of the sample.

3.3. ATOMIC FORCE MICROSCOPY

We have studied the topography and frictional properties of single layer graphene (SLG) samples on SiO_2 and mica using Atomic Force Microscopy (AFM) in the contact mode using XE-100 Atomic Force Microscope from Park Systems under ambient conditions. In all measurements, a contact mode AFM probe with a less than 10 nm tip diameter and 0.2 N/m force constant (PPP-CONTSCR from Nanosensors) were used. The force applied by the tip to the sample surface was kept between 2.5 and 3 nN. No significant differences were observed in the measured quantities under these different forces.

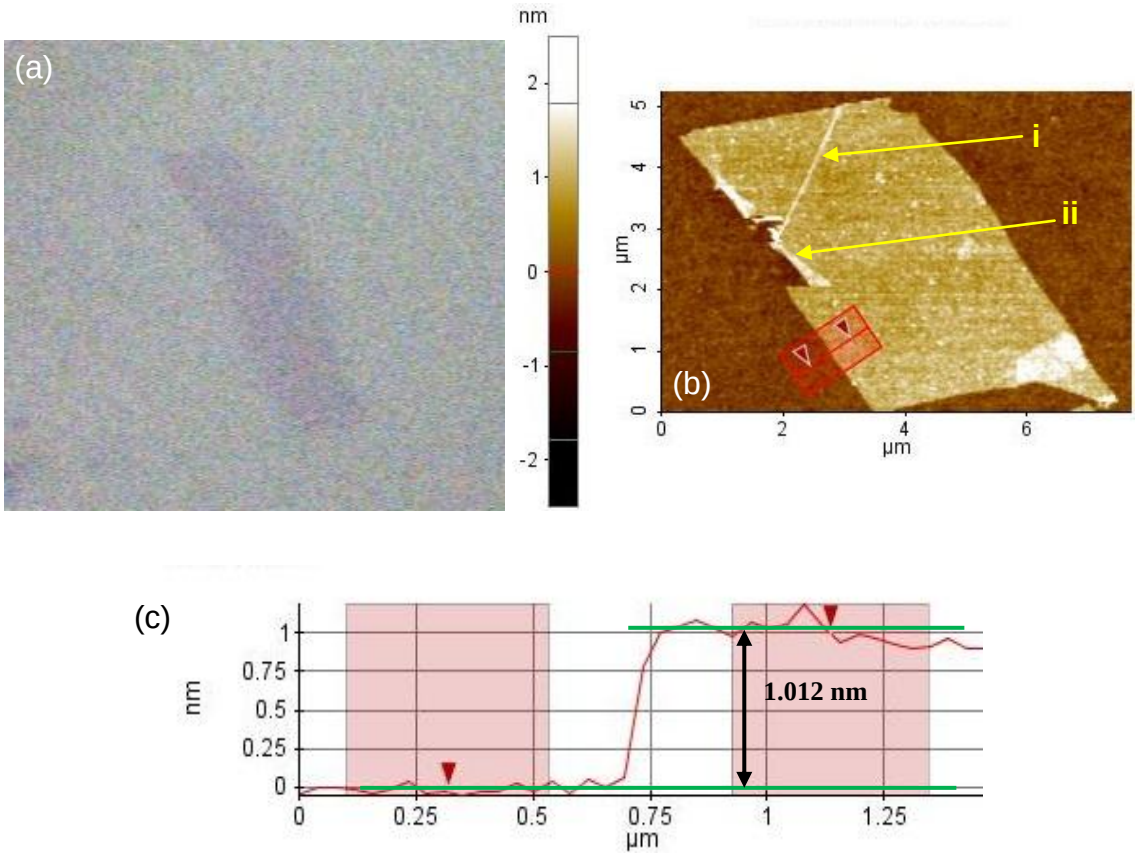

Figure 3.9 The optical (a) and topography (b) images of graphene sample on silica substrate by AFM. (c) represents the height of the graphene.

In Fig. 3.9, we show the optical and AFM topography image obtained from a SLG exfoliated on SiO_2 substrate. The AFM topography image looks different than the optical image because the lower part of the graphene was damaged by the AFM tip at the initial stages of the experiments. Lower part of the graphene sample was swept by the AFM tip to the right end of the sample as can be seen in Fig. 3.9b. In Fig. 3.9b a crease (i) on the upper left corner of the sample is visible and a backfolded graphene

piece (ii) can be seen just below this crease. These two features are probably artifacts formed either at the exfoliation stage or by the AFM tip. Although unintentional in this case, such manipulation of the graphene samples were previously performed using AFM tips in other studies and this also shows the somewhat fragile nature of the graphene samples. A more detailed image of the undamaged upper part of the sample is shown in Fig. 3.10a and 3.10b.

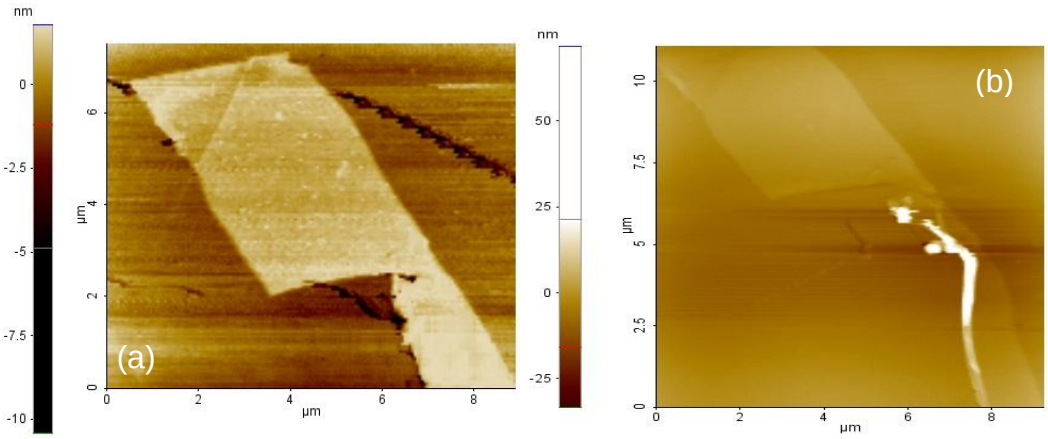

Figure 3.10 The topography image of the swept graphene by the AFM tip.

We measured the height difference between the graphene and the substrate by taking an averaged line profile (indicated by the red shaded box in Fig. 3.9c), and further averaging the graphene and silica portions of the line profile as shown in Fig. 3.9c. The height difference is measured to be approximately 1 nm, in agreement with previous measurements of SLG with AFM under ambient conditions [15]. The distance between two adjacent layers in graphite is about 3.5 Å. In fact, in situ AFM measurements of the height of graphene on SiO_2 yielded values very close to this difference. Therefore, the value obtained in air is attributed to adlayers of water or oxygen collected on the graphene or at the interfacial region between graphene and silica which desorbed in vacuum [15] A reliable roughness value can not be obtained from our measurements due to the relatively large AFM tip radius (~7 nm) and the instrumental noise which were observed to be as large as 0.5 nm in some experiments. However, typical surface roughness of SiO_2 is known approximately 1 nm.

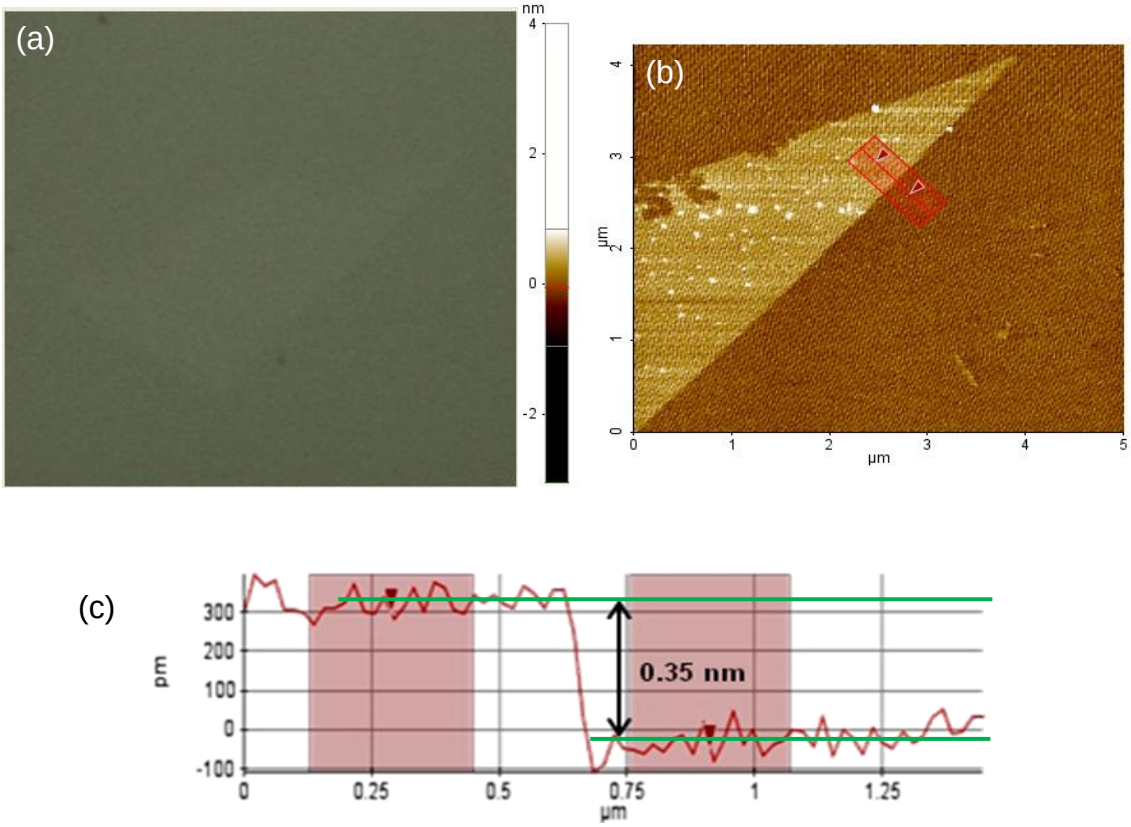

Figure 3.11 The topography images of graphene sample on mica substrate by AFM.

We collected similar topography data for graphene samples exfoliated on mica. The AFM topography image in the contact mode of the sample on mica that we also used for the Raman experiments (see Fig. 3.8) is shown in Fig. 3.11. A small graphene ribbon can be seen next to the larger single layer graphene flake. This smaller piece was not detected under the optical microscope (Fig. 3.2b) but its signatures can be seen in the Raman map shown in Fig. 3.8. Furthermore, the AFM topography image shows significant amount of structural defects around the edges of the flake. The origin of these defects are not clear to us at this point but we take it as a caution that different flakes can be very dissimilar in terms of its crystal quality. Furthermore, small specks can be seen on the graphene sample which may originate from contaminants introduced from the air or originally present on the sample. Measuring the height of the flake relative to the mica surface, we found that the height of the sample is approximately 0.35 nm. Since this value is close to graphite interlayer distance, we conclude that unlike SLG on SiO_2 where the height was measured to be 1 nm, SLG on mica is less prone to contamination. This conclusion is also supported by the Raman measurements on mica where we observed that the Raman features did not vary over different spots on

the sample whereas there were significant variations for the graphene flake on silica. The roughness of the sample and the substrate were not measured but graphene on mica is known to be atomically smooth [48]. The uniformity of the Raman signal and the close to ideal sample height might be relevant to this flat structure of the SLG on mica.

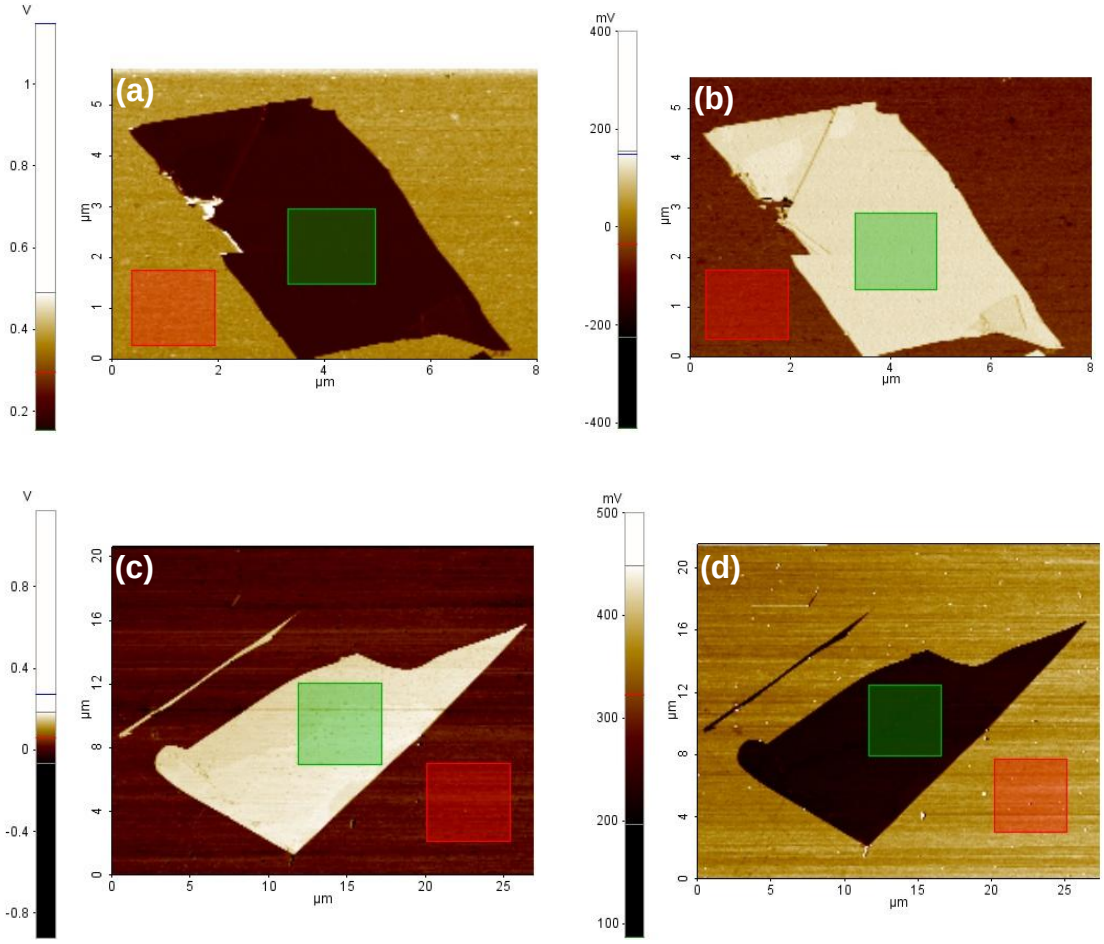

Figure 3.12 Left to right (a,c) and right to left (b,d) lateral force images of single layer graphene on silica (a,b) or mica (c,d) substrates by AFM.

During the acquisition of topography data, it is also possible to observe frictional interaction between the AFM tip and the sample. In our work, we compared the frictional forces experienced by the AFM tip during its interaction with the graphene or the substrate. We did not attempt to measure the absolute value of the frictional forces as these values may vary significantly from one AFM tip to another. Figure 3.12 shows the lateral force microscopy images of SLG samples on SiO_2 and on mica. Figure 3.12a and c show the images obtained while the AFM tip is scanning from left to right and Fig. 3.12b and d show images obtained while scanning from right to left. The data collected from opposite scan directions can be used to determine reference reading of

the instrument for zero lateral force. To compare the frictional values and to determine this zero lateral force reading we averaged the instrumental lateral force data from the PSPD measured in mV over the shaded regions shown in the images of Fig. 3.12. Since the right to left and left to right lateral forces must be equal in magnitude and opposite in direction, arithmetic average of these two values should give us the zero lateral force reading of the PSPD. Then the voltage value which is proportional to the lateral force for each region (the substrate and the sample) can be extracted by subtracting this zero lateral force value from the averaged PSPD reading of each region. Upon making such a calculation using the average values from the red and green shaded regions shown in Fig. 3.12, we determined that the frictional force on SiO_2 is approximately seven times larger than the frictional force on SLG whereas the frictional force on mica is approximately six times larger than on SLG. A reliable comparison of the frictional data from different substrate is not possible because the tip conditions can be very different. Graphene can not be used as a calibration reference either because the topography of the flakes is rough on silica and smooth on mica. The large difference in lateral forces between graphene and substrate allows us to obtain high contrast images of flakes under atomic force microscope. We found this technique to be very useful even when the instrumental noise is very high preventing us from determining the sample position using topography data.

CHAPTER 4

CONCLUSION

In this dissertation, our goal was to produce a single layer graphene sample which is known as the finest two dimensional crystalline material in the universe that humankind ever measured. In addition to this property it has also many intrinsic and intriguing features that can be used in new technological developments as a starting new area of future science. Due to the properties of graphene material that is mentioned at the beginning, we wanted to be a part of this fascinating topic in the science world by trying to find new different behaviours of graphene. In our work, we used Raman spectroscopy and Atomic Force Microscopy (AFM) to study graphene samples on SiO_2 and mica substrates.

Raman spectroscopy is a very strong tool in characterizing graphene as it can readily provide information on the number of atomic layers and the quality of the samples. On the other hand, AFM can be used to determine physical structure and also various mechanical properties (such as friction) of samples at the microscopic level. In our study, samples were prepared using the well established method of mechanical exfoliation of graphene on the desired substrate. The graphene flakes were prepared on 300 nm thick SiO_2 grown on silicon wafer and freshly cleaved mica substrates. The samples were then first inspected under the optical microscope to identify few atom thick flakes of interest which are then studied using a dispersive Raman microscope. Subsequently, the structure of the sample is investigated using contact-mode AFM and lateral force microscopy (LFM) modes.

Due to finite transmission and an optical interference effect even single atom thick graphene samples on SiO_2 can be easily discerned under optical microscope (see Fig.

3.1). Figure 3.4 illustrates Raman spectra of graphene of differing thicknesses as measured on SiO_2 substrate using a 532 nm excitation laser. The shape and the relative intensities of G and 2D peaks of graphene can be used to identify the thickness of the sample. Further the absence of D peak at 1350 cm^{-1} in our spectrum is an indication of the high quality of the samples obtained. On closer inspection, we determined that Raman peak positions shift towards lower values at the edges of the sample. To confirm that this is an edge effect a Raman map at 2677 cm^{-1} shift is provided in Figure 3.6. At this slightly off-peak location, edge signal is stronger all around the sample when compared to central regions. We attribute this shift to reduced coordination at the edge atoms and associated changes in the electronic and vibrational properties near the edge of the sample.

Under the optical microscope, the graphene flakes on mica appear brighter than the bare mica substrate. Though contrast is very small, it is still possible to optically identify single layer graphene on mica. Raman spectrum was qualitatively similar but the signal level was lower. Raman intensity map can be used to better visualize the sample.

Further characterization is performed using contact mode AFM and LFM. AFM topography measurements on both substrates were consistent with sample thicknesses determined via Raman spectroscopy. Graphene on mica is observed to be smoother than the ones on SiO_2, but the background noise prevented us from specifying a quantitative value to surface roughness in either case. We have, however, measured the frictional interaction of the AFM tip with graphene and mica surface using LFM. The frictional coefficients on graphene were found to be six times smaller than the ones on mica surface. This equipped us with yet another method for high contrast high resolution imaging of the sample.

In summary, we have prepared graphene samples with mechanical exfoliation on SiO_2 and mica substrates and then scanned the surface of these wafers under an optical microscope to determine the graphene flakes as a monolayer, bilayer or multilayer graphene. Subsequently, we took Raman measurement to confirm the graphene flakes whether they are SLG or not. Then we used the Raman Mapping technique to obtain and display the location of the graphene flakes on the substrates in order graphene flakes to be visible with a high contrast image. The samples were studied using Raman spectroscopy, and AFM. The observed shifts in Raman peak positions of the 2D mode

towards the edge of the graphene on silica is attributed to the doping of the contamination. However, we did not see any shifts in peaks for mica substrate. As a result of this, we may say that there is a uniform doping of the contaminations. We also think that doping effect corresponded to mica wafer may cancel the doping effect of the impurities on the surface. Consequently, mica is found to be smoother than graphene on SiO_2 as expected. We demonstrated that high contrast images of graphene on mica can be obtained by using both Raman imaging and LFM.

REFERENCES

[1] P.R Wallace, Phys. Rev. **71**, 622 (1947).

[2] J.W. McClure, Phys. Rev. **104**, 666 (1956).

[3] J.C. Sloczewski and P.R. Weiss, Phys. Rev. **109**, 272 (1958).

[4] R.C. Tatar and S. Rabii, Phys. Rev. B, **25**, 4126 (1982).

[5] K.S. Novoselov *et al.*, Science 306, 666 (2004).

[6] K.S. Novoselov *et al.*, Proc. Natl. Acad. Sci. **102**, 10451 (2005).

[7] Y.B. Zhang *et al.*, Nature **438**, 201 (2005).

[8] A. K. Geim and K. S. Novoselov, Nature Mat. **6**, 183 (2007).

[9] Raji Heyrovska, arXiv:0804.4086 [physics.gen-ph] (2008).

[10] Nobel Foundation announcement (2010).

[11] P. Blake *et al.*, Appl. Phys. Lett., **91**, 063124 (2007).

[12] T.A. Land *et al.*, Surf. Sci. **264**, 261 (1992).

[13] T. Ohta *et al.*, Science **313**, 951 (2006).

[14] E. Stolyarova, *et al.*, Proc. Natl. Acad. Sci. **104**, 9209 (2007).

[15] M. Ishigami, *et al.*, Nano Lett. **7**, 1643 (2007).

[16] Locatelli, Andrea, *et al.*, ACS NANO, **4**, 4879 (2010).

[17] A.C. Ferrari, *et al.*, Phys. Rev. Lett., **97**, 187401 (2006).

[18] F.Tuinstra and J. Koenig, J. Chem. Phys. **53**, 1126 (1970).

[19] A.C. Ferrari and J. Robertson, Phys. Rev. B **61**, 14095 (2000).

[20] S. Piscanec *et al*., Phys. Rev. Lett. **93**, 185503 (2004).

[21] A. Gupta, *et al.*, Nano Lett., **6**, 2667 (2006).

[22] K.I. Bolotin, *et al.*, Solid State Comm., **146**, 351 (2008).

[23] K.S. Novoselov, *et al.*, Science, **315**, 1379 (2007).

[24] K.S. Novoselov *et al.*, Nature **438**, 197 (2005).

[25] A.M.J. Schakel, Phys. Rev. D., **43**, 1428 (1991).

[26] J. Tworzydlo, *et al.*, Phys. Rev. Lett., **96**,246802 (2006).

[27] K.S. Novoselov, *et al.*, Nature Phys. **2**, 177 (2006).

[28] A. Bostwick, *et al.*, Nature Phys. **3**, 36 (2007).

[29] G.M. Rutter, *et al.*, Science, **317**, 219 (2007).

[30] K.R. Knox, *et al.*, Phys. Rev. B, **78**, 201408 (2008).

[31] F. Schedin, *et al.*, Nature Mat., **6**, 652 (2007).

[32] V. Barone, *et al.*, Nano Lett., **6**, 2748 (2006).

[33] M.Y. Han, *et al.*, Phys. Rev. Let., **98**, 206805 (2007).

[34] J. Chen, *et al.*, Adv. Mat., **19**, 3623 (2007).

[35] H. Wang, *et al.*, IEEE Elect. Device L. **30**, 547 (2009).

[36] P.Ramesh, *et al.*, J. Colloid Interface Sci., **95**, 274 (2004).

[37] Mohammad Choucair, *et al*., Nature Nanotechnology **4**, 30 (2009).

[38] http://www.media.rice.edu/media/NewsBot.asp?MODE=VIEW&ID=15057

[39] Zhengzong Sun, *et al*., Nature **468**, 549 (2010).

[40] Dmitry V. Kosynkin, *et al*., Nature **458**, 872 (2009).

[41] Ewen Smith,Geoffrey Dent, 2005, Modern Raman Spectroscopy – A Practical Approach, John Wiley & Sons Ltd, England , 0-471-49668-5.

[42] http://en.wikipedia.org/wiki/Atomic_force_microscopy, March (2011).

[43] H.G. Hansma, *et al*., Biophysical Journal **68**,1672 (1995).

[44] Roger Proksch, *et al*., Biophysical Journal **71**, 2155 (1996).

[45] R. Erlandsson, *et al*., J. Chem. Phys. **89**, 5190 (1988).

[46] C.M. Mate, *et al*., Phys. Rev. Lett. **59**, 1942 (1987).

[47] Das, A. , *et al*., Nat. Nanotechnol. **3**, 210 (2008).

[48] Chun Hung Lui, *et al*., Nature Lett.**462**, 339 (2009).